Author Manuscript

Author Manuscript

Author Manuscript

Author Manuscript

HHS Public Access

Author manuscript

J Comp Neurol. Author manuscript; available in PMC 2024 October 01.

Published in final edited form as:

J Comp Neurol. 2023 October ; 531(14): 1459–1481. doi:10.1002/cne.25525.

Organization of orbitofrontal-auditory pathways in the Mongolian gerbil

Rose Ying[1,2,3,*], **Lashaka Hamlette**[2], **Laudan Nikoobakht**[2], **Rakshita Balaji**[2], **Nicole Miko**[2], **Melissa L. Caras**[1,2,3]

[1]Neuroscience and Cognitive Science Program, University of Maryland, College Park, Maryland, 20742

[2]Department of Biology, University of Maryland, College Park, Maryland, 20742

[3]Center for Comparative and Evolutionary Biology of Hearing, University of Maryland, College Park, Maryland, 20742

Abstract

Sound perception is highly malleable, rapidly adjusting to the acoustic environment and behavioral demands. This flexibility is the result of ongoing changes in auditory cortical activity driven by fluctuations in attention, arousal, or prior expectations. Recent work suggests that the orbitofrontal cortex (OFC) may mediate some of these rapid changes, but the anatomical connections between the OFC and the auditory system are not well-characterized. Here, we used virally-mediated fluorescent tracers to map the projection from OFC to the auditory midbrain, thalamus, and cortex in a classic animal model for auditory research, the Mongolian gerbil (*Meriones unguiculatus*). We observed no connectivity between the OFC and the auditory midbrain, and an extremely sparse connection between the dorsolateral OFC and higher-order auditory thalamic regions. In contrast, we observed a robust connection between the ventral and medial subdivisions of the OFC and the auditory cortex, with a clear bias for secondary auditory cortical regions. OFC axon terminals were found in all auditory cortical lamina but were significantly more concentrated in the infragranular layers. Tissue-clearing and lightsheet microscopy further revealed that auditory cortical-projecting OFC neurons send extensive axon collaterals throughout the brain, targeting both sensory and non-sensory regions involved in learning, decision-making, and memory. These findings provide a more detailed map of orbitofrontal-auditory connections and shed light on the possible role of the OFC in supporting auditory cognition.

Keywords

Orbitofrontal cortex; Auditory cortex; Sensory processing; Top-down

[*]**Correspondence:** Rose Ying, Biology-Psychology Building, 4094 Campus Dr, College Park, MD 20742, roseying@umd.edu.

Author contributions: M.L.C, L.H., and R.Y. designed the research; R.Y., L.H., L.N., R.B., and N.M. performed the research; R.Y. and M.L.C. wrote the paper.

Author Manuscript Author Manuscript Author Manuscript Author Manuscript

Introduction

Sensory perception is critical for survival, enabling organisms to find food and mates, evade predators, and navigate to safety. To perform these behaviors successfully, individuals must parse a seemingly endless array of complex time-varying sensory stimuli and respond appropriately. Accordingly, perceptual sensitivity is highly malleable, shifting from moment to moment as a result of fluctuations in attentional state (Ahissar & Hochstein, 1993; Luck & Ford, 1998; Shinn-Cunningham, 2008; Spitzer et al., 1988; Yotsumoto & Watanabe, 2008), arousal level (Asutay & Västfjäll, 2012; Kim et al., 2017; Mather & Sutherland, 2011; McGinley et al., 2015), and expectations (Ashton, 2014; Carcea et al., 2017; de Lange et al., 2018; Pinto et al., 2015; Stein & Peelen, 2015; Vangkilde et al., 2012). These dynamics allow organisms to filter out irrelevant information, make rapid predictions about upcoming sensory events, and more easily detect, discriminate, or identify signals of high interest or value.

Perceptual flexibility results from rapid changes in stimulus-driven activity within sensory cortices. Reductions in response variability (McGinley et al., 2015; von Trapp et al., 2016), adaptive transformations of receptive field properties (Atiani et al., 2009; David et al., 2012; Fontanini & Katz, 2006; Fritz et al., 2003; Fritz et al., 2005, 2007; Yin et al., 2014), reorganizations of neuronal networks (Cohen & Maunsell, 2009; Downer et al., 2017; Francis et al., 2018, 2022; Sheikhattar et al., 2018; Steinmetz et al., 2000), and shifts in response gain (Caras & Sanes, 2017; Chapman & Meftah, 2005; Davis, 1964; Hubel et al., 1959; Niwa et al., 2012; Spitzer et al., 1988; Treue & Maunsell, 1999; Yoshida & Katz, 2011) have all been reported. Many of these rapid changes are thought to be mediated by descending inputs from frontal cortical brain regions to sensory cortices. While significant attention has been devoted to studying the contribution of medial prefrontal cortical areas (Bahmani et al., 2019; Shinn-Cunningham, 2017), a growing body of work suggests that the orbitofrontal cortex (OFC) also plays an important role. OFC is unique in that it is the only prefrontal cortical region to receive input from all sensory modalities (Le Merre et al., 2021), suggesting its central involvement in sensory processing. More recent work has revealed its role in the top-down control of sensory cortical function (Banerjee et al., 2020; Liu et al., 2020; Liu et al., 2021).

The OFC’s contribution to auditory cognition is particularly evident. OFC neurons respond to sounds (Sharma & Bandyopadhyay, 2020; Srivastava & Bandyopadhyay, 2020; Winkowski et al., 2013) and in humans, the magnitude of OFC activity predicts aspects of auditory perception and behavior. For example, increased OFC gain is associated with phantom sound perception during tinnitus (Lee et al., 2020; Vanneste et al., 2012). Conversely, OFC lesions impair tone recognition and weaken auditory cortical responsiveness (Kam et al., 2018). This latter finding, which links OFC damage to a reduction in auditory cortical activity, is consistent with studies in mice that demonstrate that OFC activation can alter sound-evoked representations in the primary auditory cortex. Specifically, pairing sounds with electrical stimulation of the OFC (Winkowski et al., 2013) or with optogenetic stimulation of OFC axon terminals in the auditory cortex (Winkowski et al., 2018) shifts the frequency tuning of auditory cortical neurons and alters auditory cortical

Author Manuscript Author Manuscript Author Manuscript Author Manuscript

network structure. These changes improve the ability of the auditory cortical neuronal population to discriminate the paired sound frequency.

While connections between the OFC and auditory regions have been identified in several species, including house mice (*Mus musculus*) (Sharma & Bandyopadhyay, 2020; Srivastava & Bandyopadhyay, 2020; Winkowski et al., 2018; Zingg et al., 2014), Lister-hooded rats (*Rattus norvegicus*) (Olthof et al., 2019), rhesus macaque monkeys (*Macaca mulatta*) (Cavada et al., 2000; Hackett et al., 1999; Romanski, Bates, et al., 1999; Romanski, Tian, et al., 1999), and humans (Cammoun et al., 2015), we lack a detailed characterization of these connections in a classic and well-established model for auditory research, the Mongolian gerbil (*Meriones unguiculatus*). Gerbils offer several unique advantages for auditory studies. Unlike other commonly used rodent models, like mice or rats, gerbils exhibit excellent low-frequency hearing capabilities, similar to humans (Ryan, 1976). Additionally, there is a large body of literature on gerbil auditory anatomy (Budinger et al., 2000a, 2000b, 2008; Budinger & Scheich, 2009; Radtke-Schuller et al., 2016), development (Anbuhl et al., 2022; Caras & Sanes, 2015, 2019; Müller, 1996; Rosen et al., 2010; Sanes, 1993; Sanes & Rubel, 1988), sound perception (Jüchter et al., 2022; von Trapp et al., 2016; Yao et al., 2020), auditory skill learning (Caras & Sanes, 2017, 2019; Sarro & Sanes, 2011; Wetzel et al., 1998), hearing loss (Henry et al., 1980; Mills et al., 1990; Takesian et al., 2012; Tucci et al., 1999; von Trapp et al., 2017; Xu et al., 2007), and central nervous system function (Amaro et al., 2021; Belliveau et al., 2014; Buran et al., 2014; Franken et al., 2018; Kreeger et al., 2021; Lesica et al., 2010; Myoga et al., 2014; Yao & Sanes, 2021), spanning multiple decades. A more complete description of the inputs from the OFC to the gerbil auditory system would facilitate our understanding of the neural circuits that support rapid adjustments to the acoustic environment, and may additionally shed light on the mechanistic link between hearing status and cognitive function (Lin et al., 2011; Taljaard et al., 2016).

Here, we used virally mediated fluorescent tracers to characterize the descending projections from the OFC to the gerbil auditory cortex, thalamus, and midbrain. We report a heterogeneous pattern of auditory connectivity across the mediolateral axis of the OFC. Dorsolateral OFC (DLO) sends a sparse projection to the auditory thalamus and exhibits little to no connectivity with the auditory midbrain or cortex. In contrast, ventral (VO) and medial (MO) subdivisions of the OFC innervate primary auditory cortex (Au1) as well as the secondary dorsal (AuD) and ventral (AuV) cortices, with the densest labeling in the deep infragranular layers. Further investigation using tissue clearing and lightsheet microscopy revealed that auditory cortical-projection neurons also send collaterals to distant targets, including non-auditory sensory cortices and brain regions implicated in learning, decision-making, and memory. Together, our findings reveal the organization of orbitofrontal-auditory connectivity in the gerbil brain and provide additional anatomical context for the OFC's contribution to auditory cognition.

Materials and methods

Animals:

Mongolian gerbils were obtained from Charles River and bred in-house. Gerbils were group housed on a 12-hour light cycle and given *ad libitum* access to chow (Purina Mills Lab Diet

Author Manuscript Author Manuscript Author Manuscript Author Manuscript

5001) and water. All procedures except one were conducted at the University of Maryland College Park, and were approved by the University of Maryland Institutional Animal Care and Use Committee. The remaining single procedure (subject ID_269953, see Table 1) was conducted at New York University and was approved by the New York University Institutional Animal Care and Use Committee.

Viral injections:

Subjects were injected with one or more viral tracers into the OFC, or into subcortical or cortical auditory regions. Viruses were injected at two depths in auditory cortical regions to ensure spread across cortical layers. Our injections were performed with the animal's head level between bregma and lambda, rather than between lambda and the occipital ridge, as in Radtke-Schuller et al., 2016. Therefore, our reported anterior-posterior target coordinates differ from those of Radtke-Schuller and colleagues. For complete details about each injection, including the virus, injection volume, titer, and coordinates used, see Table 1.

A total of 44 animals (aged postnatal day 58-637) were used in this study. The data from off-target injections (N = 10), injections with excessive virus spread outside the region of interest (N = 5), and brains with excessive tissue damage (N = 2) were excluded from all analyses. Therefore, this report includes data from 27 animals (N = 16 female).

One day prior to surgery, animals were given meloxicam (1.5 mg/kg, 1.5 mg/mL) either via oral suspension or subcutaneous injection or a carprofen medigel cup as a preventative analgesic. On the day of surgery, animals were administered meloxicam or carprofen and dexamethasone (0.35 mg/kg, 0.5 mg/mL) subcutaneously to prevent edema. Subjects were placed in a small induction chamber in which isoflurane (5%) was continuously administered in O_2 (2 L/min). After the animal was sedated, the fur on the animal's head was shaved. The animal was then transferred to a warming pad on a stereotaxic device (Kopf) and secured in place with ear bars and a bite bar. A nose cone delivered a steady flow of isoflurane (1.5-2.5%) and oxygen at a flow rate of 2 L/min. Once a surgical plane of anesthesia was achieved (as evidenced by slow and steady respiration, and the absence of a toe-pinch response) ophthalmic ointment was applied to the eyes, and the surgical area was treated with alternating applications of betadine and alcohol. A midline incision was made, and the skin and fascia were retracted. The skull was cleaned and dried with H_2O_2 and a craniotomy was made over the region of interest using a 5mm drill bit. A glass injection pipette was filled with mineral oil and attached to a programmable injector (Nanoject III, Drummond). The virus was drawn up into the tip and positioned over the injection site. A durotomy was performed, and the pipette was inserted to the targeted depth. The virus was injected at a rate of 2 nL/sec and allowed to diffuse for 5-15 mins prior to pipette retraction. The craniotomy was covered with KwikSil and the skin was sutured along the incision. Immediately after the surgery, subjects were given a subcutaneous injection of Normosol (1-2 mL) and allowed to recover in their home cage. An additional dose of meloxicam or carprofen and dexamethasone were administered 24 hours after surgery, and subjects were closely monitored after the surgical procedure.

Author Manuscript Author Manuscript Author Manuscript Author Manuscript

Histology:

Subjects remained in their home cages for 3-5 weeks after injections to allow for protein expression, after which animals were perfused for histology. Animals were anesthetized with an intraperitoneal injection of ketamine (150 mg/kg, 25 mg/mL) and xylazine (6 mg/kg, 1 mg/mL) or sodium pentobarbital (60-100 mg/kg, 50 mg/mL) in saline. After the subject was determined to be unresponsive to a toe pinch, the chest cavity was opened and the subject was perfused transcardially using 1x phosphate buffered saline (PBS) followed by 4% paraformaldehyde.

Tissue processing and confocal microscopy:

Extracted brains were post-fixed in 4% paraformaldehyde at 4°C for at least one day, then embedded in 6% agar and sliced on a vibratome (Leica VT1000 S) at 70 μm thickness. Slices were mounted on gelatin subbed slides and dried overnight. Mounted sections were counterstained with NeuroTrace 435/455 Fluorescent Nissl (Invitrogen N21479). The slices were rehydrated with 1x PBS for at least 30 minutes. After a 5-minute wash in 1x PBS, the slices were incubated in 1x PBS with 0.1% Triton X for 20 minutes. The slides were washed three times for 5 minutes each in 1x PBS, then incubated in a 1:100 NeuroTrace dilution overnight at 4°C. After incubation, the slices were washed for 10 minutes in 1x PBS with 0.1% triton, then twice in 1x PBS for 5 minutes each. The slides were then cover-slipped using ProLong Diamond Antifade Mountant and imaged using a confocal microscope (Zeiss LSM 980). Post-processing, including stitching and z-stack processing, were completed using Zeiss ZEN and FIJI software (Schindelin et al., 2012).

Tissue clearing and lightsheet microscopy:

For lightsheet imaging experiments, fixed brains were extracted, packaged in 1x PBS with 0.02% sodium azide and sent to LifeCanvas Technologies in Cambridge, MA. Brains were cleared using SHIELD (Park et al., 2019) and delipified using Clear+ reagents (LifeCanvas Technologies). The mCherry signal was enhanced with eFLASH (Yun et al., 2019) in a SmartBatch+ device (LifeCanvas Technologies) using a primary rabbit anti-RFP antibody (7.5 μg, Rockland, 600-401-379, RRID: AB_11182807) and a secondary donkey anti-rabbit IgG (H+L) antibody (15 μg, biotium, 20178, RRID: AB_10854111). Brains were then incubated overnight at 37°C in 50% EasyIndex (Refractive Index = 1.52, LifeCanvas Technologies) followed by 24 hour incubation in 100% EasyIndex. Whole brains were imaged using a SmartSPIM axially-swept lightsheet microscope at 3.6X magnification. Regions of particular interest were imaged again at 15X magnification. Clearing and image acquisition was performed by LifeCanvas Technologies.

Cell body quantification in OFC:

Brain sections separated by 250-300μm along the rostral to caudal dimension were imaged. Each image was matched to a section in the brain atlas (Radtke-Schuller et al., 2016). The emergence of the claustrum distinguished anterior OFC (plates 8-11 in Radtke-Schuller et al., 2016) from posterior OFC (plates 12-16 in Radtke-Schuller et al., 2016), consistent with previous reports in rodents (Barreiros et al., 2021a; Barreiros et al., 2021b). Manual counts of labeled cells were performed for each image, and cell counts were independently verified

Author Manuscript Author Manuscript Author Manuscript Author Manuscript

by another lab member. To determine whether the proportion of labeled cells differed between hemispheres, cell counts in each hemisphere were normalized to the total number of labeled cells across both hemispheres. To determine whether the proportion of labeled cells differed among different OFC subregions, labeled cells in each ipsilateral subregion were normalized to the total number of labeled cells within the ipsilateral hemisphere. For complete details about cell counts and corresponding plate numbers in the gerbil brain atlas, see Table 2.

Fiber analysis in the auditory cortex:

Intensity analysis was performed using FIJI. For each image, color channels were split into red, green, and blue, and the appropriate channel was converted to grayscale (red for turboRFP, green for EGFP). Excess background was removed using the Subtract Background and Subtract functions. The regions of interest were identified by comparing the Nissl stain and other gross morphological features to the gerbil brain atlas (Radtke-Schuller et al., 2016) and marked on the image. Intensity values were calculated using the Plot Profile tool along linear transects, drawn from the cortical surface through the cortical layers at roughly equal distances through the region of interest. Custom MATLAB code was written to bin intensity values (200 bins per sample) as a function of transect length. Intensity values were then normalized to the maximum intensity value for each image. For each subject, one image was taken in the anterior portion of the auditory cortex (plates 28-30 in the gerbil brain atlas) and one image from the posterior portion (plates 31-33). To compare between anterior and posterior sections, each set of anterior and posterior images was processed so that the intensity histogram range, median, and standard deviation between images were as similar as possible.

Axon collateral analysis:

Lightsheet images were reconstructed into a 3-D model in Imaris Viewer. Using anatomical borders and landmarks, we identified brain regions that exhibited labeled fibers in both subjects. The relative density of labeling within each brain region was manually categorized as either weak (+), moderate (++), or strong (+++) (Table 7). For representative examples of each density category, see Fig. S1.

Statistical analysis:

For analysis of cell bodies in the OFC, generalized linear mixed models (GLMs) and paired t-tests were performed in JMP Pro 15. Subject and subregion were included as nested categorical random effects (subregion within subject). To quantify the intensity of fiber labeling throughout the auditory cortex, we used R to construct a GLM using the ‘glmmTMB’ (Brooks et al., 2017), DHARMa (Hartig, 2022), car (Fox & Weisberg, 2018), and emmeans (Lenth, 2023) packages. Subject, region (AuD/Au1/AuV), layer (1-6), and position (anterior/posterior) were included as categorical random effects and quadruple nested (position within layer within region within subject). Normal distribution of residuals was tested after running the GLM and an analysis of variance (ANOVA) was used to analyze the statistical significance of the GLM. Post-hoc pairwise comparisons were conducted after transforming data back to the original scale.

Author Manuscript Author Manuscript Author Manuscript Author Manuscript

We considered results statistically significant when $p < 0.05$. All p values were adjusted for multiple comparisons using a Bonferroni correction and were corrected for any violations of sphericity using the Greenhouse-Geisser method.

Results

Retrograde tracing from core auditory cortex

A previous study reported the presence of retrogradely labeled cell bodies in the OFC after small injections of fluorescent dextran tracers were delivered to gerbil Au1, but the distribution pattern of labeled soma within the OFC was not reported (Budinger et al., 2008). Rodent OFC is classically divided into distinct subregions along its mediolateral axis, including the dorsolateral/agranular insular (DLO/AI), lateral (LO), ventral (VO), and medial (MO) areas (Krettek & Price, 1977; Üngür & Price, 2000; Price, 2006; Ray & Price, 1992; Rempel-Clower, 2007). These subdivisions exhibit different patterns of anatomical connectivity, and are thought to mediate distinct behavioral and cognitive functions (for review see Barreiros et al., 2021a; Bradfield & Hart, 2020; Izquierdo, 2017; Rempel-Clower, 2007). These observations raise the question of whether the OFC neurons that innervate the auditory cortex are evenly distributed across the mediolateral axis, or primarily originate in one or more discrete subregions.

To answer this question, we injected AAVrg-hSyn-EGFP, a viral vector in a serotype that allows for robust retrograde access to long-range projection neurons (Tervo et al., 2016), into left core auditory cortex. Correctly placed injections (N = 8; see Table 1) were centered in Au1 and/or the anterior auditory field (AAF) and spanned multiple cortical layers (Figure 1a, b). In two cases, the injection site exhibited minimal upward spread, just beyond the border with secondary somatosensory cortex (S2) and AuD; in the remaining cases the injections were contained entirely within the boundaries of Au1/AAF.

To first confirm that our retrograde tracing approach worked as expected, we took advantage of the known interhemispheric connection between auditory cortices (Budinger et al., 2000a; Diamond et al., 1968; Imig & Reale, 1980), and examined the contralateral auditory cortex for the presence of labeled cell bodies. As expected, we observed many brightly labeled neurons throughout the contralateral auditory cortex (Figure 1c).

In the OFC, we observed clearly labeled cell bodies scattered throughout the region (Figure 1d). A significantly higher proportion of the labeled neuron population was in the ipsilateral hemisphere compared to the contralateral hemisphere ($t_7 = -4.80$, $p = 0.002$) (Figure 1e). Given that the proportion of contralateral labeled neurons was significantly smaller, we focused our subsequent analyses on the ipsilateral hemisphere only. Within the ipsilateral hemisphere, cell body labeling was unevenly distributed across OFC subregions (GLM, $F_{3,28} = 45.31$, $p < 0.0001$; Figure 1f). The highest proportion of labeled cell bodies was consistently observed in the VO, followed by MO. Very little labeling was evident in LO or DLO/AI. A complete statistical breakdown of these results is provided in Table 3.

Author Manuscript Author Manuscript Author Manuscript Author Manuscript

Retrograde tracing from secondary auditory cortices

Non-sensory processes, like attention and behavioral context, modulate the activity of higher-order auditory regions, and the magnitude of these modulations are often larger than those observed in Au1 (Atiani et al., 2014; Jäncke et al., 1999; Niwa et al., 2015; O'Sullivan et al., 2019; Yin et al., 2020). This finding suggests that non-sensory brain regions may differentially connect to primary and secondary auditory cortices. We therefore asked whether OFC neurons project to two secondary auditory cortical regions in the gerbil —the dorsal (AuD) and ventral (AuV) auditory cortices.

First, we injected a retrograde tracer (AAVrg-hSyn-EGFP) into the left AuD. Well-placed injections (N = 3) spanned most or all cortical layers and exhibited little to no spread beyond the boundaries of AuD (Figure 2a, b). As expected, we identified cell bodies in the contralateral AuD, confirming the efficacy of retrograde expression (Figure 2c) (Budinger et al., 2000a). An examination of OFC revealed brightly labeled cell bodies densely clustered in the ventral portion of the region (Figure 2d). Similar to Au1-projecting neurons, the vast majority of AuD-projecting neurons were located in the ipsilateral hemisphere ($t_2 = 7.81$, $p = 0.016$; Figure 2e).

We then quantified apparent differences in cell body labeling across the mediolateral axis of the ipsilateral OFC. Labeled neurons were unequally distributed across OFC subregions (GLM, $F_{3,8} = 655.64$, $p < 0.0001$), and the pattern was similar to that observed for Au1/AAF-projecting neurons: VO contained the highest proportion of labeled cell bodies, followed by MO, LO, and DLO/AI (Figure 2f). A complete statistical breakdown of these results is provided in Table 4.

We also injected retrograde tracers (AAVrg-hSyn-EGFP or AAVrg-CAG-tdTomato) into the AuV. Injections (N = 4) were centered in AuV, with one injection exhibiting minor spread upwards into AuD (Figure 3a, b). We identified cell bodies in the contralateral AuV to confirm the efficacy of the retrograde virus (Figure 3c) (Budinger et al., 2000a). As in Au1 and AuD, cell bodies were present in the OFC, with a significantly higher proportion of cells on the ipsilateral side ($t_2 = 3.29$, $p = 0.047$; Figure 3d, e). Across the mediolateral axis, we once again observed unequal distribution of labeled neurons (GLM, $F_{3,12} = 62.35$, $p < 0.0001$; Figure 3f). VO contained the highest proportion of labeled cells, followed by MO, LO, and DLO. A complete statistical breakdown of these results is provided in Table 5.

Qualitatively, we observed that more OFC cell bodies were present after retrograde tracing from secondary auditory cortices than from Au1 (e.g., compare Figures 1d, 2d, and 3d). These results were not quantified due to uneven sample sizes across groups and variability in injection spread across cortical layers.

Retrograde tracing from the auditory thalamus and midbrain

Subcortical auditory regions, including the medial geniculate nucleus (MGN) and inferior colliculus (IC), also play important roles in sound processing, cognition, and multi-modal integration (Bartlett & Wang, 2007; Brainard & Knudsen, 1993; Ehret & Merzenich, 1988; Wang et al., 2008). Both of these structures exhibit context-dependent modulations of sound-evoked responses (Franceschi & Barkat, 2021; Gilad et al., 2020; Gruters & Groh,

Author Manuscript Author Manuscript Author Manuscript Author Manuscript

2012; Mihai et al., 2021; Ryan et al., 1984; Ryan & Miller, 1977; Slee & David, 2015; von Kriegstein et al., 2008), and the activation of prefrontal cortex shapes neural activity in the MGN (Barry et al., 2017). These findings suggest that direct inputs from frontal cortical areas may influence subcortical auditory processing. In line with this idea, one previous study reported that neurons in the ventral and lateral OFC innervate the central nucleus of the rat IC (Olthof et al., 2019). These observations led us to ask whether a similar connection exists between the OFC and the gerbil IC and/or MGN.

Towards that end, we injected a retrograde tracer (AAVrg-hSyn-eGFP) into the left MGN of three subjects. Viral expression was primarily localized to the ventral subdivision of the MGN (MGV), which serves as the primary lemniscal input to Au1 (Budinger et al., 2000b), but exhibited some spread into the nearby non-lemniscal dorsal (MGD) subdivision and the medial zone of the medial geniculate (MZMG) (Figure 4a, b). To confirm retrograde expression, we documented labeled cell bodies in the IC, which provides the majority of ascending input to the MGN (Cant & Benson, 2007; Hackett, 2011; Kudo & Niimi, 1978; Ledoux et al., 1987; Morest, 1965) (Figure 4c).

Two of the three MGN injections resulted in sparse cell body labeling in the OFC, primarily in the ipsilateral DLO/AI (Figure 4d). The remaining injection did not result in any OFC cell body labeling. Notably, this injection was entirely confined to the MGV, with no spread into non-lemniscal areas (see purple striped injection pattern in Figure 4a). These data suggest that MGN-projecting neurons in the OFC primarily terminate in higher-order auditory thalamic subdivisions. Because these injections resulted in relatively few labeled cell bodies in the OFC, we did not quantify these findings.

To investigate whether OFC projects to 1C, we injected four animals with AAVrg-hSyn-eGFP into the left 1C. All injections were centered in the central nucleus of the 1C (CIC), which serves as the primary ascending input to the MGV (Hackett, 2011; Morest, 1965), with moderate spread into the overlying external and dorsal IC cortices (Figure 5a,b). As expected from decades of previous work characterizing a prominent corticofugal pathway from Au1 to IC (Bajo et al., 2010; Bajo & Moore, 2005; Budinger et al., 2000b; Cooper & Young, 1976; Games & Winer, 1988; Suga et al., 2000; Williamson & Polley, 2019) we observed distinct cell body labeling in layer 5 of Au1 (Figure 5c). Despite this confirmation of successful retrograde cortical expression, and in contrast to an earlier report in rat (Olthof et al., 2019), no cell bodies were observed in any of the OFC subregions in either hemisphere (Figure 5d).

Anterograde tracing from OFC

Context-dependent changes in sound-evoked activity exhibit a distinct laminar profile in the auditory cortex (Atencio & Schreiner, 2010; Franceschi & Barkat, 2021; Francis et al., 2018; O'Connell et al., 2014; Sugimoto et al., 1997). Determining the pattern of OFC innervation across auditory cortical layers could therefore provide insight into the potential functional role of the OFC in guiding sound-driven behavior. We injected an anterograde tracer (AAV1-hSyn-TurboRFP) into the left OFC of four animals to confirm our retrograde tracing results and to characterize the translaminar pattern of OFC axon distribution in the gerbil auditory cortex. Well-placed injections were centered within the boundaries of OFC

Author Manuscript Author Manuscript Author Manuscript Author Manuscript

(generally LO and VO), with minimal upward spread into the prelimbic and motor cortices and/or downward spread into the piriform cortex (Figure 6a, b).

As shown in Figure 6c, brightly labeled fibers were observed in both primary (Au1) and secondary (AuD and AuV) auditory cortices, and the labeling intensity differed significantly across these regions (GLM/ANOVA, $X^2(2) = 22.87$, $p < 0.0001$) (Figure 6d, e). Post-hoc tests revealed that overall label intensity was similar in AuD and AuV ($t_{103} = 0.517$, $p = 0.8632$), and significantly stronger in both regions compared to Au1 (AuD: $t_{103} = 3.514$, $p = 0.0019$; AuV: $t_{103} = 3.206$, $p = 0.005$). These findings indicate that OFC neurons preferentially target higher-order auditory cortical areas over Au1, consistent with our qualitative retrograde tracing observations. Fiber labeling intensity significantly differed overall across cortical layers (GLM/ANOVA, $\chi^2(5) = 119.0933$, $p < 0.0001$; Figure 6d, e). Post-hoc tests showed that in contrast to the relatively sparse fibers observed in superficial and granular layers, the infragranular layers (5 and 6) exhibited robust labeling. A full statistical breakdown of these results is provided in Table 6. There was no significant difference in terminal intensity along the anterior-posterior axis (GLM/ANOVA, $\chi^2(1) = 0.3890$, $p = 0.5328$; not shown).

Our retrograde tracing experiments revealed a sparse connection between the OFC and MGN (Figure 4) and no connection between OFC and IC (Figure 5). To determine whether these observations are genuine, or whether they instead reflect a limited ability of the AAV-retro serotype to access corticothalamic and corticocollicular projections (Tervo et al. 2016), we asked whether anterogradely labeled axon fibers were present in the MGN and/or IC of subjects injected with AAV1-hSyn-TurboRFP into the OFC. In line with our retrograde findings, three injections resulted in sparse labeling throughout the MGN (Figure 7a), with the fourth animal excluded as images were not taken of subcortical auditory areas in this subject. These findings confirm that OFC does in fact innervate MGN, albeit weakly. No clear labeling was observed in the IC (Figure 7b).

Auditory cortical-projecting neurons in the OFC send axon collateral to other brain regions

Individual frontal cortical neurons often project to multiple downstream targets, consistent with their role in coordinating brain-wide activity (Gao et al., 2022). To gain insight into how the OFC might specifically orchestrate sound-guided behavior, we asked whether Au1-projecting neurons in the OFC also send axon collaterals to other brain regions. To do so, we injected left Au1 with a virus to drive retrograde expression of Cre-recombinase (AAVrg-hSyn-Cre) and injected left OFC with a virus to drive Cre-dependent expression of mCherry (AAV1-hSyn-DIO-mCherry) in two animals (see Table 1). This intersectional viral strategy selectively labels just the OFC neurons that project to Au1, along with their axon collaterals. We then used tissue clearing and lightsheet microscopy to look for the presence of mCherry fluorescence throughout the intact gerbil brain. In both injected subjects, we observed a dense cluster of brightly labeled cell bodies localized to the ipsilateral OFC (primarily VO and LO; Figure 8a, b), and three distinct axon tracts emanating from these neurons (Figure 8c-f).

One tract extended dorsally, through the ipsilateral caudate putamen (Figure 9a, b) and through the external capsule to various cortical regions, including the cingulate cortex

Author Manuscript Author Manuscript Author Manuscript Author Manuscript

(Figure 9a, c), somatosensory cortex (Figure 9a, d), auditory cortex (Figure 9e, f), and visual cortex (Figure 9g, h). Within these regions, collaterals targeted multiple cortical layers, and higher-magnification imaging revealed en passant boutons in all regions and terminal boutons in auditory cortex and visual cortex, indicating probable synapses. Additional areas of notable fiber labeling stemming from this axon tract include prelimbic cortex, retrosplenial cortex, and parietal cortex, although we did not confirm the presence of boutons in these regions.

A second axon tract traveled ventrally to the ipsilateral parahippocampal region (Figure 8c-f). Fibers were observed in the ectorhinal, perirhinal, and entorhinal cortices (Figure 9e, g, i, j), and particularly dense labeling was observed in the subiculum (Figure 9i, k). These fibers exhibited en passant and terminal boutons, suggesting the presence of functional synapses.

A final axon tract crossed the midline and then branched extensively, targeting the contralateral OFC, cingulate cortex, caudate putamen, auditory cortex, and parahippocampal region (Figure 8c, d). A complete list of regions where we observed labeled fibers, along with a qualitative estimate of the intensity of labeling is provided in Table 7.

Discussion

Using anterograde and retrograde AAV tracers, we characterized the descending projections from the OFC to cortical and subcortical auditory regions in an established model organism for auditory research, the Mongolian gerbil. We found that the OFC exhibits little to no connectivity with the MGN and IC, but robustly innervates auditory cortices. The pattern of connectivity varied across OFC's mediolateral axis, such that nearly all auditory cortical-projecting neurons were observed in the ventral and medial subdivisions. These neurons preferentially targeted infragranular layers, with the densest innervation in secondary auditory cortices. An intersectional viral strategy, tissue clearing, and lightsheet microscopy further revealed that the OFC neurons that project to the auditory cortex also send wide-ranging axon collaterals to distant targets, including many non-sensory areas. Our results provide an anatomical basis for understanding the role of the OFC in shaping auditory function and sound-guided behavior.

We observed a very sparse connection between the dorsolateral OFC and MGN, and no connectivity between OFC and IC. While our findings are broadly consistent with prior rodent work (Allen Mouse Brain Connectivity Atlas, experiments 158435116, 112423392; Hoover & Vertes, 2011), they stand in contrast to a recent study that reported the presence of labeled cell bodies in the OFC after retrograde tracers were injected into the IC (Olthof et al., 2019). One possible explanation for this discrepancy is methodological: Olthof and colleagues used retrograde beads to label connections, whereas we relied on AAV-mediated tract tracing. AAV efficiency can vary considerably across species and cell types (for reviews see Haery et al., 2019; Saleeba et al., 2019) and the retrograde virus we used has limited access to some corticocollicular pathways (Tervo et al., 2016). We therefore confirmed the absence of an OFC-IC connection via anterograde tracing with an AAV1 serotype. AAV1 is commonly used for anterograde targeting (Saleeba et al., 2019) including

Author Manuscript Author Manuscript Author Manuscript Author Manuscript

in the gerbil (Kotak et al., 2017; Masri et al., 2023; Mowery et al., 2017), and successfully labels projections from the OFC to other midbrain regions (Babalian et al., 2019; Benavidez et al., 2021). We therefore believe that the discrepancy between our results and those of Olthof et al. is likely explained by species-specific anatomical differences.

In Au1, we found OFC axons in all cortical layers, suggesting that OFC is well-positioned to directly shape sensory-evoked responses throughout the cortical column. Indeed, optogenetic stimulation of OFC axon terminals in mice activates multiple Au1 laminae and alters L2/3 receptive fields (Winkowski et al., 2018). Our data suggest that OFC's influence on Au1 sound processing may be largely mediated via infragranular activation, as OFC fiber innervation is strongest in L5/6. Neurons in L5/6 provide extensive feedback to subcortical auditory structures (for review see Winer, 2006), and make local connections within Au1 (Guo et al., 2017; Onodera & Kato, 2022; Prieto & Winer, 1999; Williamson & Polley, 2019). These pathways shape spectrotemporal tuning and response gain in the inferior colliculus, medial geniculate body, and auditory cortex (Antunes & Malmierca, 2021; Gao & Suga, 1998; Ma & Suga, 2001; Malmierca et al., 2015; Saldeitis et al., 2021; Zhang & Yan, 2008), and directly impact behavioral performance on auditory detection and discrimination tasks (Guo et al., 2017; Homma et al., 2017). In addition, layer 6 corticothalamic circuits have been hypothesized to gate the transmission of behaviorally-relevant information from the periphery to the cortex (He, 1997; Sherman & Koch, 1986; Yu et al., 2004; Zhang et al., 1997). Taken together, these findings suggest that OFC may mediate rapid changes in stimulus salience by activating both intracortical and subcortical feedback projections originating in the deep layers of auditory cortex. Future experiments examining OFC's impact on auditory cortical infragranular activity *in vivo* are needed, as prior reports have exclusively monitored and/or manipulated OFC axon terminals in L2/3 (Liu et al., 2021; Winkowski et al., 2018).

Sound-evoked representations are transformed as they traverse the auditory cortical hierarchy, gradually incorporating information about stimulus meaning or emotional valence as the signals move from primary to secondary and tertiary regions (Atiani et al., 2014; Elgueda et al., 2019; Grosso et al., 2015; Takahashi et al., 2010, 2011; Yin et al., 2020). Our finding that OFC sends a larger projection to secondary auditory cortical regions than to Au1 suggests one anatomical basis for these observations. Higher-order auditory regions also exhibit stimulus-evoked activity that persists for hundreds of milliseconds after sound offset (Atiani et al., 2014; Elgueda et al., 2019) and long temporal integration windows (Bendor & Wang, 2007; Boemio et al., 2005; Scott et al., 2011), both of which offer an increased opportunity for signals encoding behavioral outcomes to be combined with sensory input. These findings, coupled with VO's proposed role in signaling reward history, prediction error, and value (Riceberg & Shapiro, 2017; Steiner & Redish, 2012; Stolyarova & Izquierdo, 2017; Young & Shapiro, 2011), suggest that OFC's robust projection to secondary auditory cortices may serve to rapidly update sensory representations during sound-guided behavior. Recent work suggests that OFC inputs to primary sensory cortical regions may also serve a similar function (Banerjee et al., 2020; Liu et al., 2020; Liu et al., 2021).

Author Manuscript Author Manuscript Author Manuscript Author Manuscript

We found that auditory cortical-projecting OFC neurons also send wide-ranging axon collaterals to various brain regions involved in learning, memory, and decision making. One downstream target that receives substantial collateral innervation is a striatal area strongly implicated in auditory behavior—the posterior portion of the caudate putamen (CPu). The posterior CPu receives direct projections from Au1 (Budinger et al., 2000a, 2008; Roger & Arnault, 1989), and these inputs support associative learning by integrating information about sound identity, behavioral choice, and expectation of reward (Guo et al., 2018, 2019; Xiong et al., 2015; Znamenskiy & Zador, 2013). These findings have led some to hypothesize that many of the response properties exhibited by the posterior CPu are inherited directly from Au1 (Guo et al., 2019). Our results suggest an alternative, though not mutually exclusive, model in which Au1 and posterior CPu exhibit similar responses in part because they receive input from the same OFC neurons. It is also interesting to note that within the CPu, the pattern of Au1 innervation matches the pattern of innervation from axon collaterals branching from the OFC to Au1 projection (Budinger et al., 2000b; Roger & Arnault, 1989). Taken together, these results suggest that Au1 and OFC may work in tandem to generate stable striatal representations of learned stimulus values during sound-guided behavior.

We also observed a significant collateral projection to the parahippocampal region, which is comprised of entorhinal, ectorhinal, and perirhinal cortices, as well as the subiculum. These structures are critical for working memory (Nemanic et al., 2004; Young et al., 1997). Though the anatomical connection between the OFC and the parahippocampal region is well documented (Burwell & Amaral, 1998; Hoover & Vertes, 2011; Kondo & Witter, 2014; Witter et al., 2017), our understanding of the function of this pathway is limited. OFC, sensory cortices, and the parahippocampal region all display stimulus-selective activity when sensory stimuli are held in working memory (Gottlieb et al., 1989; Ramus & Eichenbaum, 2000; Young et al., 1997). Our observation that the same OFC neurons that project to the auditory cortex also project to the parahippocampal region suggests that these neurons are particularly well-positioned to coordinate activity between these two areas during working memory. Future experiments employing targeted manipulations of OFC axon terminals will be needed to reveal whether these pathways do indeed form part of a sensory mnemonic circuit.

Collectively, our data reveal a long-range projection from the OFC that is particularly well-positioned to rapidly update stimulus representations in the gerbil auditory cortex and orchestrate brain-wide changes during auditory learning. These findings advance our understanding of the neural circuits that support auditory cognition and perceptual flexibility.

Supplementary Material

Refer to Web version on PubMed Central for supplementary material.

Acknowledgements:

This work was supported by National Institute of Health Grant K99/R00DC016046 to M.L.C and T32DC00046 to R.Y. Purchase of the Zeiss LSM 980 Airyscan 2 was supported by Award Number 1S10OD025223-01A1 from

Author Manuscript Author Manuscript Author Manuscript Author Manuscript

the National Institute of Health. We thank Dr. Dan Sanes (New York University) for the use of his lab for one of the reported procedures. We also thank Dr. Daniel Stolzberg (University of Maryland) for help with image processing, Dr. Daniel Miller (University of Illinois at Urbana-Champaign) for advice on data analysis, Dr. Matheus Macedo-Lima (University of Maryland) for help with statistics, Taylor Thomas for help with surgeries, and all members of the M.L.C. laboratory for their constructive criticism and support. The authors declare no competing financial interests.

Abbreviations

AAF	Anterior auditory field
AuD	Dorsal auditory cortex
AuV	Ventral auditory cortex
Au1	Primary auditory cortex
CIC	Central nucleus of the inferior colliculus
Cg	Cingulate cortex
CPu	Caudate putamen (striatum)
DCIC	Dorsal cortex of the inferior colliculus
DLO/AI	Dorsolateral orbitofrontal cortex/agranular insular cortex
DMIC	Dorsomedial nucleus of the inferior colliculus
ECIC	External cortex of the inferior colliculus
Ect	Ectorhinal cortex
Ent	Entorhinal cortex
IC	Inferior colliculus
LO	Lateral orbitofrontal cortex
PRh	Perirhinal cortex
MGN	Medial geniculate nucleus
MGD	Medial geniculate nucleus, dorsal part
MGM	Medial geniculate nucleus, medial part
MGV	Medial geniculate nucleus, ventral part
MZMG	Marginal zone of the medial geniculate
MO	Medial orbitofrontal cortex
Sub	Subiculum translational area
S1	Primary somatosensory cortex
S2	Secondary somatosensory cortex

Author Manuscript Author Manuscript Author Manuscript Author Manuscript

OFC	Orbitofrontal cortex
VO	Ventral orbitofrontal cortex
V1	Primary visual cortex
V2	Secondary visual cortex

References

Ahissar M, & Hochstein S (1993). Attentional control of early perceptual learning. Proceedings of the National Academy of Sciences of the United States of America, 90(12), 5718–5722.Allen Reference Atlas – Mouse Brain Connectivity [brain atlas]. Available from connectivity.brain-map.org. [PubMed: 8516322]

Amaro D, Ferreiro DN, Grothe B, & Pecka M (2021). Source identity shapes spatial preference in primary auditory cortex during active navigation. Current Biology, 31(17), 3875–3883. [PubMed: 34192513]

Anbuhl KL, Yao JD, Hotz RA, Mowery TM, & Sanes DH (2022). Auditory processing remains sensitive to environmental experience during adolescence in a rodent model. Nature Communications, 13(1), 2872.

Antunes FM, & Malmierca MS (2021). Corticothalamic Pathways in Auditory Processing: Recent Advances and Insights From Other Sensory Systems. Frontiers in Neural Circuits, 15.

Ashton RH (2014). "Nothing Good Ever Came from New Jersey": Expectations and the Sensory Perception of Wines. Journal of Wine Economics, 9(3), 304–319.

Asutay E, & Västfjäll D (2012). Perception of Loudness Is Influenced by Emotion. PLOS ONE, 7(6), e38660. [PubMed: 22685594]

Atencio CA, & Schreiner CE (2010). Laminar Diversity of Dynamic Sound Processing in Cat Primary Auditory Cortex. Journal of Neurophysiology, 103(1), 192–205. [PubMed: 19864440]

Atiani S, David SV, Elgueda D, Locastro M, Radtke-Schuller S, Shamma SA, & Fritz JB (2014). Emergent Selectivity for Task-Relevant Stimuli in Higher-Order Auditory Cortex. Neuron, 82(2), 486–499. [PubMed: 24742467]

Atiani S, Elhilali M, David SV, Fritz JB, & Shamma SA (2009). Task difficulty and performance induce diverse adaptive patterns in gain and shape of primary auditory cortical receptive fields. Neuron, 61(3), 467–480. [PubMed: 19217382]

Babalian A, Eichenberger S, Bilella A, Girard F, Szabolcsi V, Roccaro D, Alvarez-Bolado G, Xu C, & Celio MR (2019). The orbitofrontal cortex projects to the parvafox nucleus of the ventrolateral hypothalamus and to its targets in the ventromedial periaqueductal grey matter. Brain Structure and Function, 224(1), 293–314. 10.1007/s00429-018-1771-5 [PubMed: 30315416]

Bahmani Z, Clark K, Merrikhi Y, Mueller A, Pettine W, Isabel Vanegas M, Moore T, & Noudoost B (2019). Prefrontal Contributions to Attention and Working Memory. Current Topics in Behavioral Neurosciences, 41, 129–153. [PubMed: 30739308]

Bajo VM, & Moore DR (2005). Descending projections from the auditory cortex to the inferior colliculus in the gerbil, Meriones unguiculatus. Journal of Comparative Neurology, 486(2), 101–116. [PubMed: 15844210]

Bajo VM, Nodal FR, Moore DR, & King AJ (2010). The descending corticocollicular pathway mediates learning-induced auditory plasticity. Nature Neuroscience, 13(2), 253–260. [PubMed: 20037578]

Banerjee A, Parente G, Teutsch J, Lewis C, Voigt FF, & Helmchen F (2020). Value-guided remapping of sensory cortex by lateral orbitofrontal cortex. Nature, 585(7824), 245–250. [PubMed: 32884146]

Barreiros IV, Ishii H, Walton ME, & Panayi MC (2021). Defining an orbitofrontal compass: Functional and anatomical heterogeneity across anterior-posterior and medial-lateral axes. Behavioral Neuroscience, 135(2), 165–173. [PubMed: 34060873]

Author Manuscript Author Manuscript Author Manuscript Author Manuscript

Barreiros IV, Panayi MC, & Walton ME (2021). Organization of Afferents along the Anterior–posterior and Medial–lateral Axes of the Rat Orbitofrontal Cortex. Neuroscience, 460, 53–68. [PubMed: 33609638]

Barry KM, Robertson D, & Mulders WHAM (2017). Medial geniculate neurons show diverse effects in response to electrical stimulation of prefrontal cortex. Hearing Research, 353, 204–212. [PubMed: 28709732]

Bartlett EL, & Wang X (2007). Neural representations of temporally modulated signals in the auditory thalamus of awake primates. Journal of Neurophysiology, 97(2), 1005–1017. [PubMed: 17050830]

Belliveau LAC, Lyamzin DR, & Lesica NA (2014). The Neural Representation of Interaural Time Differences in Gerbils Is Transformed from Midbrain to Cortex. Journal of Neuroscience, 34(50), 16796–16808. [PubMed: 25505332]

Benavidez NL, Bienkowski MS, Zhu M, Garcia LH, Fayzullina M, Gao L, Bowman I, Gou L, Khanjani N, Cotter KR, Korobkova L, Becerra M, Cao C, Song MY, Zhang B, Yamashita S, Tugangui AJ, Zingg B, Rose K, … Dong H-W (2021). Organization of the inputs and outputs of the mouse superior colliculus. Nature Communications, 12(1), Article 1. 10.1038/s41467-021-24241-2

Bendor D, & Wang X (2007). Differential neural coding of acoustic flutter within primate auditory cortex. Nature Neuroscience, 10(6), 763–771. [PubMed: 17468752]

Boemio A, Fromm S, Braun A, & Poeppel D (2005). Hierarchical and asymmetric temporal sensitivity in human auditory cortices. Nature Neuroscience, 8(3), 389–395. [PubMed: 15723061]

Bradfield LA, & Hart G (2020). Rodent medial and lateral orbitofrontal cortices represent unique components of cognitive maps of task space. Neuroscience & Biobehavioral Reviews, 108, 287–294. [PubMed: 31743727]

Brainard MS, & Knudsen EI (1993). Experience-dependent plasticity in the inferior colliculus: A site for visual calibration of the neural representation of auditory space in the barn owl. Journal of Neuroscience, 13(11), 4589–4608. [PubMed: 8229186]

Brooks ME, Kristensen K, Benthem KJ van, Magnusson A, Berg CW, Nielsen A, Skaug HJ, Mächler M, & Bolker BM (2017). GlmmTMB Balances Speed and Flexibility Among Packages for Zero-inflated Generalized Linear Mixed Modeling. The R Journal, 9(2), 378–400.

Budinger E, Heil P, & Scheich H (2000a). Functional organization of auditory cortex in the Mongolian gerbil (Meriones unguiculatus). III. Anatomical subdivisions and corticocortical connections. European Journal of Neuroscience, 12(7), 2425–2451. [PubMed: 10947821]

Budinger E, Heil P, & Scheich H (2000b). Functional organization of auditory cortex in the Mongolian gerbil (Meriones unguiculatus). IV. Connections with anatomically characterized subcortical structures. European Journal of Neuroscience, 12(7), 2452–2474. [PubMed: 10947822]

Budinger E, Laszcz A, Lison H, Scheich H, & Ohl FW (2008). Non-sensory cortical and subcortical connections of the primary auditory cortex in Mongolian gerbils: Bottom-up and top-down processing of neuronal information via field AI. Brain Research, 1220, 2–32. [PubMed: 17964556]

Budinger E, & Scheich H (2009). Anatomical connections suitable for the direct processing of neuronal information of different modalities via the rodent primary auditory cortex. Hearing Research, 258(1), 16–27. [PubMed: 19446016]

Buran BN, von Trapp G, & Sanes DH (2014). Behaviorally Gated Reduction of Spontaneous Discharge Can Improve Detection Thresholds in Auditory Cortex. Journal of Neuroscience, 34(11), 4076–4081. [PubMed: 24623785]

Burwell RD, & Amaral DG (1998). Cortical afferents of the perirhinal, postrhinal, and entorhinal cortices of the rat. Journal of Comparative Neurology, 398(2), 179–205. [PubMed: 9700566]

Cammoun L, Thiran JP, Griffa A, Meuli R, Hagmann P, & Clarke S (2015). Intrahemispheric corticocortical connections of the human auditory cortex. Brain Structure & Function, 220(6), 3537–3553. [PubMed: 25173473]

Cant NB, & Benson CG (2007). Multiple topographically organized projections connect the central nucleus of the inferior colliculus to the ventral division of the medial geniculate nucleus in the gerbil, Meriones unguiculatus. Journal of Comparative Neurology, 503(3), 432–453. [PubMed: 17503483]

Author Manuscript Author Manuscript Author Manuscript Author Manuscript

Caras ML, & Sanes DH (2015). Sustained Perceptual Deficits from Transient Sensory Deprivation. Journal of Neuroscience, 35(30), 10831–10842. [PubMed: 26224865]

Caras ML, & Sanes DH (2017). Top-down modulation of sensory cortex gates perceptual learning. Proceedings of the National Academy of Sciences, 114(37), 9972–9977.

Caras ML, & Sanes DH (2019). Neural Variability Limits Adolescent Skill Learning. Journal of Neuroscience, 39(15), 2889–2902. [PubMed: 30755494]

Carcea I, Insanally MN, & Froemke RC (2017). Dynamics of auditory cortical activity during behavioural engagement and auditory perception. Nature Communications, 8(1), 14412.

Cavada C, Compañy T, Tejedor J, Cruz-Rizzolo RJ, & Reinoso-Suárez F (2000). The anatomical connections of the macaque monkey orbitofrontal cortex. A review. Cerebral Cortex (New York, N.Y.: 1991), 10(3), 220–242. [PubMed: 10731218]

Chapman CE, & Meftah E-M (2005). Independent Controls of Attentional Influences in Primary and Secondary Somatosensory Cortex. Journal of Neurophysiology, 94(6), 4094–4107. [PubMed: 16148278]

Cohen MR, & Maunsell JHR (2009). Attention improves performance primarily by reducing interneuronal correlations. Nature Neuroscience, 12(12), 1594–1600. [PubMed: 19915566]

Cooper MH, & Young PA (1976). Cortical projections to the inferior colliculus of the cat. Experimental Neurology, 51(2), 488–502. [PubMed: 1269575]

David SV, Fritz JB, & Shamma SA (2012). Task reward structure shapes rapid receptive field plasticity in auditory cortex. Proceedings of the National Academy of Sciences of the United States of America, 109(6), 2144–2149. [PubMed: 22308415]

Davis H (1964). Enhancement of Evoked Cortical Potentials in Humans Related to a Task Requiring a Decision. Science (New York, N.Y.), 145(3628), 182–183. [PubMed: 14171564]

de Lange FP, Heilbron M, & Kok P (2018). How Do Expectations Shape Perception? Trends in Cognitive Sciences, 22(9), 764–779. [PubMed: 30122170]

Diamond IT, Jones EG, & Powell TPS (1968). Interhemispheric fiber connections of the auditory cortex of the cat. Brain Research, 11(1), 177–193. [PubMed: 5722715]

Downer JD, Rapone B, Verhein J, O'Connor KN, & Sutter ML (2017). Feature-Selective Attention Adaptively Shifts Noise Correlations in Primary Auditory Cortex. Journal of Neuroscience, 37(21), 5378–5392. [PubMed: 28432139]

Ehret G, & Merzenich MM (1988). Complex sound analysis (frequency resolution, filtering and spectral integration) by single units of the inferior colliculus of the cat. Brain Research Reviews, 13(2), 139–163.

Elgueda D, Duque D, Radtke-Schuller S, Yin P, David SV, Shamma SA, & Fritz JB (2019). State-dependent encoding of sound and behavioral meaning in a tertiary region of the ferret auditory cortex. Nature Neuroscience, 22(3), 447–459. [PubMed: 30692690]

Fontanini A, & Katz DB (2006). State-Dependent Modulation of Time-Varying Gustatory Responses. Journal of Neurophysiology, 96(6), 3183–3193. [PubMed: 16928791]

Fox J, & Weisberg S (2018). An R Companion to Applied Regression (3rd edition). SAGE Publications, Inc.

Franceschi GD, & Barkat TR (2021). Task-induced modulations of neuronal activity along the auditory pathway. Cell Reports, 37(11), 110115. [PubMed: 34910908]

Francis NA, Mukherjee S, Koçillari L, Panzeri S, Babadi B, & Kanold PO (2022). Sequential transmission of task-relevant information in cortical neuronal networks. Cell Reports, 39(9), 110878. [PubMed: 35649366]

Francis NA, Winkowski DE, Sheikhattar A, Armengol K, Babadi B, & Kanold PO (2018). Small Networks Encode Decision-Making in Primary Auditory Cortex. Neuron, 97(4), 885–897. [PubMed: 29398362]

Franken TP, Joris PX, & Smith PH (2018). Principal cells of the brainstem's interaural sound level detector are temporal differentiators rather than integrators. ELife, 7, e33854. [PubMed: 29901438]

Fritz JB, Elhilali M, & Shamma SA (2005). Differential Dynamic Plasticity of A1 Receptive Fields during Multiple Spectral Tasks. Journal of Neuroscience, 25(33), 7623–7635. [PubMed: 16107649]

Author Manuscript Author Manuscript Author Manuscript Author Manuscript

Fritz JB, Elhilali M, & Shamma SA (2007). Adaptive changes in cortical receptive fields induced by attention to complex sounds. Journal of Neurophysiology, 98(4), 2337–2346. [PubMed: 17699691]

Fritz J, Shamma S, Elhilali M, & Klein D (2003). Rapid task-related plasticity of spectrotemporal receptive fields in primary auditory cortex. Nature Neuroscience, 6(11), 1216–1223. [PubMed: 14583754]

Games KD, & Winer JA (1988). Layer V in rat auditory cortex: Projections to the inferior colliculus and contralateral cortex. Hearing Research, 34(1), 1–25. [PubMed: 3403382]

Gao E, & Suga N (1998). Experience-dependent corticofugal adjustment of midbrain frequency map in bat auditory system. Proceedings of the National Academy of Sciences, 95(21), 12663–12670.

Gao L, Liu S, Gou L, Hu Y, Liu Y, Deng L, Ma D, Wang H, Yang Q, Chen Z, Liu D, Qiu S, Wang X, Wang D, Wang X, Ren B, Liu Q, Chen T, Shi X, … Yan J (2022). Single-neuron projectome of mouse prefrontal cortex. Nature Neuroscience, 25(4), 515–529. [PubMed: 35361973]

Gilad A, Maor I, & Mizrahi A (2020). Learning-related population dynamics in the auditory thalamus. ELife, 9, e56307. [PubMed: 32639231]

Gottlieb Y, Vaadia E, & Abeles M (1989). Single unit activity in the auditory cortex of a monkey performing a short term memory task. Experimental Brain Research, 74(1), 139–148. [PubMed: 2924831]

Grosso A, Cambiaghi M, Renna A, Milano L, Roberto Merlo G, Sacco T, & Sacchetti B (2015). The higher order auditory cortex is involved in the assignment of affective value to sensory stimuli. Nature Communications, 6, 8886.

Gruters K, & Groh J (2012). Sounds and beyond: Multisensory and other non-auditory signals in the inferior colliculus. Frontiers in Neural Circuits, 6.

Guo L, Walker WI, Ponvert ND, Penix PL, & Jaramillo S (2018). Stable representation of sounds in the posterior striatum during flexible auditory decisions. Nature Communications, 9(1), 1534.

Guo L, Weems JT, Walker WI, Levichev A, & Jaramillo S (2019). Choice-Selective Neurons in the Auditory Cortex and in Its Striatal Target Encode Reward Expectation. Journal of Neuroscience, 39(19), 3687–3697. [PubMed: 30837264]

Guo W, Clause AR, Barth-Maron A, & Polley DB (2017). A corticothalamic circuit for dynamic switching between feature detection and discrimination. Neuron, 95(1), 180–194. [PubMed: 28625486]

Hackett TA (2011). Information flow in the auditory cortical network. Hearing Research, 271(1), 133–146. [PubMed: 20116421]

Hackett TA, Stepniewska I, & Kaas JH (1999). Prefrontal connections of the parabelt auditory cortex in macaque monkeys. Brain Research, 817(1–2), 45–58. [PubMed: 9889315]

Haery L, Deverman BE, Matho KS, Cetin A, Woodard K, Cepko C, Guerin KI, Rego MA, Ersing I, Bachle SM, Kamens J, & Fan M (2019). Adeno-Associated Virus Technologies and Methods for Targeted Neuronal Manipulation. Frontiers in Neuroanatomy, 13. https://www.frontiersin.org/articles/10.3389/fnana.2019.00093

Hartig F (2022). *DHARMa: Residual Diagnostics for Hierarchical (Multi-Level / Mixed) Regression Models* [R]. Version 0.4.6. https://CRAN.R-project.org/package=DHARMa.

He J (1997). Modulatory effects of regional cortical activation on the onset responses of the cat medial geniculate neurons. Journal of Neurophysiology, 77(2), 896–908. [PubMed: 9065857]

Henry KR, McGinn MD, & Chole RA (1980). Age-related auditory loss in the Mongolian gerbil. Archives of Oto-Rhino-Laryngology, 228(4),

Homma NY, Happel MFK, Nodal FR, Ohl FW, King AJ, & Bajo VM (2017). A Role for Auditory Corticothalamic Feedback in the Perception of Complex Sounds. Journal of Neuroscience, 37(25), 6149–6161. [PubMed: 28559384]

Hoover WB, & Vertes RP (2011). Projections of the medial orbital and ventral orbital cortex in the rat. Journal of Comparative Neurology, 519(18), 3766–3801. [PubMed: 21800317]

Hubel DH, Henson CO, Rupert A, & Galambos R (1959). Attention units in the auditory cortex. Science, 129(3358), 1279–1280. [PubMed: 13658956]

Imig TJ, & Reale RA (1980). Patterns of cortico-cortical connections related to tonotopic maps in cat auditory cortex. Journal of Comparative Neurology, 192(2), 293–332. [PubMed: 7400400]

Author Manuscript Author Manuscript Author Manuscript Author Manuscript

Izquierdo A (2017). Functional Heterogeneity within Rat Orbitofrontal Cortex in Reward Learning and Decision Making. Journal of Neuroscience, 37(44), 10529–10540. [PubMed: 29093055]

Jäncke L, Mirzazade S, & Shah NJ (1999). Attention modulates activity in the primary and the secondary auditory cortex: A functional magnetic resonance imaging study in human subjects. Neuroscience Letters, 266(2), 125–128. [PubMed: 10353343]

Jüchter C, Beutelmann R, & Klump GM (2022). Speech sound discrimination by Mongolian gerbils. Hearing Research, 418, 108472. [PubMed: 35276418]

Kam JWY, Solbakk AK, Funderud I, Endestad T, Meling TR, & Knight RT (2018). Orbitofrontal damage reduces auditory sensory response in humans. Cortex; a Journal Devoted to the Study of the Nervous System and Behavior, 101, 309–312. [PubMed: 29455945]

Kim D, Lokey S, & Ling S (2017). Elevated arousal levels enhance contrast perception. Journal of Vision, 17(2), 1–10.

Kondo H, & Witter MP (2014). Topographic organization of orbitofrontal projections to the parahippocampal region in rats. Journal of Comparative Neurology, 522(4), 772–793. [PubMed: 23897637]

Kotak VC, Mirallave A, Mowery TM, & Sanes DH (2017). GABAergic inhibition gates excitatory LTP in perirhinal cortex. Hippocampus, 27(12), 1217–1223. 10.1002/hipo.22799 [PubMed: 28881444]

Kreeger LJ, Connelly CJ, Mehta P, Zemelman BV, & Golding NL (2021). Excitatory cholecystokinin neurons of the midbrain integrate diverse temporal responses and drive auditory thalamic subdomains. Proceedings of the National Academy of Sciences, 118(10), e2007724118.

Krettek JE, & Price JL (1977). Projections from the amygdaloid complex to the cerebral cortex and thalamus in the rat and cat. Journal of Comparative Neurology, 172(4), 687–722. [PubMed: 838895]

Kudo M, & Niimi K (1978). Ascending projections of the inferior colliculus onto the medial geniculate body in the cat studied by anterograde and retrograde tracing techniques. Brain Research, 155(1), 113–117. [PubMed: 688004]

Le Merre P, Ährlund-Richter S, & Carlén M (2021). The mouse prefrontal cortex: Unity in diversity. Neuron, 109(12), 1925–1944. [PubMed: 33894133]

Ledoux JE, Ruggiero DA, Forest R, Stornetta R, & Reis DJ (1987). Topographic organization of convergent projections to the thalamus from the inferior colliculus and spinal cord in the rat. Journal of Comparative Neurology, 264(1), 123–146. [PubMed: 2445791]

Lee SY, Choi BY, Koo JW, De Ridder D, & Song JJ (2020). Cortical Oscillatory Signatures Reveal the Prerequisites for Tinnitus Perception: A Comparison of Subjects With Sudden Sensorineural Hearing Loss With and Without Tinnitus. Frontiers in Neuroscience, 14, 596647. [PubMed: 33328868]

Lenth RV (2023). *R package emmeans: Estimated marginal means* [R]. Version 1.8.5. https://cran.r-project.org/web/packages/emmeans/index.html

Lesica NA, Lingner A, & Grothe B (2010). Population Coding of Interaural Time Differences in Gerbils and Barn Owls. Journal of Neuroscience, 30(35), 11696–11702. [PubMed: 20810890]

Lin FR, Metter EJ, O'Brien RJ, Resnick SM, Zonderman AB, & Ferrucci L (2011). Hearing Loss and Incident Dementia. Archives of Neurology, 68(2), 214–220. [PubMed: 21320988]

Liu D, Deng J, Zhang Z, Zhang ZY, Sun YG, Yang T, & Yao H (2020). Orbitofrontal control of visual cortex gain promotes visual associative learning. Nature Communications, 11(1), 2784.

Liu Y, Xin Y, & Xu NL (2021). A cortical circuit mechanism for structural knowledge-based flexible sensorimotor decision-making. Neuron, 109(12), 2009–2024. [PubMed: 33957065]

Luck SJ, & Ford MA (1998). On the role of selective attention in visual perception. Proceedings of the National Academy of Sciences, 95(3), 825–830.

Ma X, & Suga N (2001). Corticofugal modulation of duration-tuned neurons in the midbrain auditory nucleus in bats. Proceedings of the National Academy of Sciences of the United States of America, 98(24), 14060–14065. [PubMed: 11707597]

Malmierca MS, Anderson LA, & Antunes FM (2015). The cortical modulation of stimulus-specific adaptation in the auditory midbrain and thalamus: A potential neuronal correlate for predictive coding. Frontiers in Systems Neuroscience, 9, 19. [PubMed: 25805974]

Author Manuscript Author Manuscript Author Manuscript Author Manuscript

Masri S, Fair R, Mowery TM, & Sanes DH (2023). Developmental hearing loss-induced perceptual deficits are rescued by cortical expression of GABAB receptors (p. 2023.01.10.523440). bioRxiv. 10.1101/2023.01.10.523440

Mather M, & Sutherland MR (2011). Arousal-biased competition in perception and memory. Perspectives on Psychological Science: A Journal of the Association for Psychological Science, 6(2), 114–133. [PubMed: 21660127]

McGinley MJ, David SV, & McCormick DA (2015). Cortical Membrane Potential Signature of Optimal States for Sensory Signal Detection. Neuron, 87(1), 179–192. [PubMed: 26074005]

Mihai PG, Tschentscher N, & von Kriegstein K (2021). Modulation of the Primary Auditory Thalamus When Recognizing Speech with Background Noise. Journal of Neuroscience, 41(33), 7136–7147. [PubMed: 34244362]

Mills JH, Schmiedt RA, & Kulish LF (1990). Age-related changes in auditory potentials of mongolian gerbil. Hearing Research, 46(3), 201–210. [PubMed: 2394633]

Morest DK (1965). The laminar structure of the medial geniculate body of the cat. Journal of Anatomy, 99(1), 143–160. [PubMed: 14245341]

Mowery TM, Penikis KB, Young SK, Ferrer CE, Kotak VC, & Sanes DH (2017). The Sensory Striatum Is Permanently Impaired by Transient Developmental Deprivation. Cell Reports, 19(12), 2462–2468. 10.1016/j.celrep.2017.05.083 [PubMed: 28636935]

Müller M (1996). The cochlear place-frequency map of the adult and developing mongolian gerbil. Hearing Research, 94(1), 148–156. [PubMed: 8789820]

Myoga MH, Lehnert S, Leibold C, Felmy F, & Grothe B (2014). Glycinergic inhibition tunes coincidence detection in the auditory brainstem. Nature Communications, 5(1), 3790.

Nemanic S, Alvarado MC, & Bachevalier J (2004). The Hippocampal/Parahippocampal Regions and Recognition Memory: Insights from Visual Paired Comparison versus Object-Delayed Nonmatching in Monkeys. Journal of Neuroscience, 24(8), 2013–2026. [PubMed: 14985444]

Niwa M, Johnson JS, O'Connor KN, & Sutter ML (2012). Active engagement improves primary auditory cortical neurons' ability to discriminate temporal modulation. Journal of Neuroscience, 32(27), 9323–9334. [PubMed: 22764239]

Niwa M, O'Connor KN, Engall E, Johnson JS, & Sutter ML (2015). Hierarchical effects of task engagement on amplitude modulation encoding in auditory cortex. Journal of Neurophysiology, 113(1), 307–327. [PubMed: 25298387]

O'Connell MN, Barczak A, Schroeder CE, & Lakatos P (2014). Layer Specific Sharpening of Frequency Tuning by Selective Attention in Primary Auditory Cortex. Journal of Neuroscience, 34(49), 16496–16508. [PubMed: 25471586]

Olthof BM, Rees A, & Gartside SE (2019). Multiple non-auditory cortical regions innervate the auditory midbrain. Journal of Neuroscience. 39(45), 8916–8928. [PubMed: 31541020]

Öngür D, & Price JL (2000). The Organization of Networks within the Orbital and Medial Prefrontal Cortex of Rats, Monkeys and Humans. Cerebral Cortex, 10(3), 206–219. [PubMed: 10731217]

Onodera K, & Kato HK (2022). Translaminar recurrence from layer 5 suppresses superficial cortical layers. Nature Communications, 13(1), 2585.

O'Sullivan J, Herrero J, Smith E, Schevon C, McKhann GM, Sheth SA, Mehta AD, & Mesgarani N (2019). Hierarchical Encoding of Attended Auditory Objects in Multi-talker Speech Perception. Neuron, 104(6), 1195–1209. [PubMed: 31648900]

Park YG, Sohn CH, Chen R, McCue M, Yun DH, Drummond GT, Ku T, Evans NB, Oak HC, Trieu W, Choi H, Jin X, Lilascharoen V, Wang J, Truttmann MC, Qi HW, Ploegh HL, Golub TR, Chen SC, … Chung K (2019). Protection of tissue physicochemical properties using polyfunctional crosslinkers. Nature Biotechnology, 37(1), Article 1. 10.1038/nbt.4281

Pinto Y, van Gaal S, de Lange FP, Lamme VAF, & Seth AK (2015). Expectations accelerate entry of visual stimuli into awareness. Journal of Vision, 15(8), 13.

Price JL (2006). Architectonic structure of the orbital and medial prefrontal cortex. In Zald D & Rauch S (Eds.), The Orbitofrontal Cortex (p. 3–18). Oxford University Press.

Prieto JJ, & Winer JA (1999). Layer VI in cat primary auditory cortex: Golgi study and sublaminar origins of projection neurons. Journal of Comparative Neurology, 404(3), 332–358. [PubMed: 9952352]

Author Manuscript Author Manuscript Author Manuscript Author Manuscript

Radtke-Schuller S, Schuller G, Angenstein F, Grosser OS, Goldschmidt J, & Budinger E (2016). Brain atlas of the Mongolian gerbil (Meriones unguiculatus) in CT/MRI-aided stereotaxic coordinates. Brain Structure & Function, 221 Suppl 1, 1–272.

Ramus SJ, & Eichenbaum H (2000). Neural Correlates of Olfactory Recognition Memory in the Rat Orbitofrontal Cortex. Journal of Neuroscience, 20(21), 8199–8208. [PubMed: 11050143]

Ray JP, & Price JL (1992). The organization of the thalamocortical connections of the mediodorsal thalamic nucleus in the rat, related to the ventral forebrain-prefrontal cortex topography. Journal of Comparative Neurology, 323(2), 167–197. [PubMed: 1401255]

Rempel-Clower NL (2007). Role of orbitofrontal cortex connections in emotion. Annals of the New York Academy of Sciences, 1121, 72–86. [PubMed: 17846152]

Riceberg JS, & Shapiro ML (2017). Orbitofrontal Cortex Signals Expected Outcomes with Predictive Codes When Stable Contingencies Promote the Integration of Reward History. Journal of Neuroscience, 37(8), 2010–2021. [PubMed: 28115481]

Roger M, & Arnault P (1989). Anatomical study of the connections of the primary auditory area in the rat. Journal of Comparative Neurology, 287(3), 339–356. [PubMed: 2778109]

Romanski LM, Bates JF, & Goldman-Rakic PS (1999). Auditory belt and parabelt projections to the prefrontal cortex in the rhesus monkey. Journal of Comparative Neurology, 403(2), 141–157. [PubMed: 9886040]

Romanski LM, Tian B, Fritz J, Mishkin M, Goldman-Rakic PS, & Rauschecker JP (1999). Dual streams of auditory afferents target multiple domains in the primate prefrontal cortex. Nature Neuroscience, 2(12), 1131–1136. [PubMed: 10570492]

Rosen MJ, Semple MN, & Sanes DH (2010). Exploiting Development to Evaluate Auditory Encoding of Amplitude Modulation. Journal of Neuroscience, 30(46), 15509–15520. [PubMed: 21084606]

Ryan AF, Miller JM, Pfingst BE, & Martin GK (1984). Effects of reaction time performance on single-unit activity in the central auditory pathway of the rhesus macaque. Journal of Neuroscience, 4(1), 298–308. [PubMed: 6693945]

Ryan A, & Miller J (1977). Effects of behavioral performance on single-unit firing patterns in inferior colliculus of the rhesus monkey. Journal of Neurophysiology, 40(4), 943–956. [PubMed: 407335]

Saldeitis K, Jeschke M, Budinger E, Ohl FW, & Happel MFK (2021). Laser-Induced Apoptosis of Corticothalamic Neurons in Layer VI of Auditory Cortex Impact on Cortical Frequency Processing. Frontiers in Neural Circuits, 15.

Saleeba C, Dempsey B, Le S, Goodchild A, & McMullan S (2019). A Student's Guide to Neural Circuit Tracing. Frontiers in Neuroscience, 13. https://www.frontiersin.org/articles/10.3389/fnins.2019.00897

Sanes DH (1993). The development of synaptic function and integration in the central auditory system. Journal of Neuroscience, 13(6), 2627–2637. [PubMed: 8501528]

Sanes DH, & Rubel EW (1988). The ontogeny of inhibition and excitation in the gerbil lateral superior olive. Journal of Neuroscience, 8(2), 682–700. [PubMed: 3339433]

Sarro EC, & Sanes DH (2011). The cost and benefit of juvenile training on adult perceptual skill. Journal of Neuroscience, 31, 5383–5391. [PubMed: 21471373]

Schindelin J, Arganda-Carreras I, Frise E, Kaynig V, Longair M, Pietzsch T, Preibisch S, Rueden C, Saalfeld S, Schmid B, Tinevez J-Y, White DJ, Hartenstein V, Eliceiri K, Tomancak P, & Cardona A (2012). Fiji: An open-source platform for biological-image analysis. Nature Methods, 9(7), 676–682. [PubMed: 22743772]

Scott BH, Malone BJ, & Semple MN (2011). Transformation of Temporal Processing Across Auditory Cortex of Awake Macaques. Journal of Neurophysiology, 105(2), 712. [PubMed: 21106896]

Sharma S, & Bandyopadhyay S (2020). Differential Rapid Plasticity in Auditory and Visual Responses in the Primarily Multisensory Orbitofrontal Cortex. ENeuro, 7(3), ENEURO.0061-20.2020.

Sheikhattar A, Miran S, Liu J, Fritz JB, Shamma SA, Kanold PO, & Babadi B (2018). Extracting neuronal functional network dynamics via adaptive Granger causality analysis. Proceedings of the National Academy of Sciences, 115(17), E3869–E3878.

Sherman SM, & Koch C (1986). The control of retinogeniculate transmission in the mammalian lateral geniculate nucleus. Experimental Brain Research, 63(1), 1–20. [PubMed: 3015651]

Author Manuscript Author Manuscript Author Manuscript Author Manuscript

Shinn-Cunningham B (2017). Cortical and Sensory Causes of Individual Differences in Selective Attention Ability Among Listeners With Normal Hearing Thresholds. Journal of Speech, Language, and Hearing Research, 60(10), 2976–2988.

Shinn-Cunningham BG (2008). Object-based auditory and visual attention. Trends in Cognitive Sciences, 12(5), 182–186. [PubMed: 18396091]

Slee SJ, & David SV (2015). Rapid Task-Related Plasticity of Spectrotemporal Receptive Fields in the Auditory Midbrain. Journal of Neuroscience, 35(38), 13090–13102. [PubMed: 26400939]

Spitzer H, Desimone R, & Moran J (1988). Increased attention enhances both behavioral and neuronal performance. Science (New York, N.Y.), 240(4850), 338–340. [PubMed: 3353728]

Srivastava HK, & Bandyopadhyay S (2020). Parallel Lemniscal and Non-Lemniscal Sources Control Auditory Responses in the Orbitofrontal Cortex (OFC). ENeuro, 7(5), ENEURO.0121-20.2020.

Stein T, & Peelen MV (2015). Content-specific expectations enhance stimulus detectability by increasing perceptual sensitivity. Journal of Experimental Psychology. General, 144(6), 1089–1104. [PubMed: 26460783]

Steiner AP, & Redish AD (2012). The Road Not Taken: Neural Correlates of Decision Making in Orbitofrontal Cortex. Frontiers in Neuroscience, 6, 131. [PubMed: 22973189]

Steinmetz PN, Roy A, Fitzgerald PJ, Hsiao SS, Johnson KO, & Niebur E (2000). Attention modulates synchronized neuronal firing in primate somatosensory cortex. Nature, 404(6774), 187–190. [PubMed: 10724171]

Stolyarova A, & Izquierdo A (2017). Complementary contributions of basolateral amygdala and orbitofrontal cortex to value learning under uncertainty. ELife, 6, e27483. [PubMed: 28682238]

Suga N, Gao E, Zhang Y, Ma X, & Olsen JF (2000). The corticofugal system for hearing: Recent progress. Proceedings of the National Academy of Sciences, 97(22), 11807–11814.

Sugimoto S, Sakurada M, Horikawa J, & Taniguchi I (1997). The columnar and layer-specific response properties of neurons in the primary auditory cortex of Mongolian gerbils. Hearing Research, 112(1), 175–185. [PubMed: 9367240]

Takahashi H, Funamizu A, Mitsumori Y, Kose H, & Kanzaki R (2010). Progressive plasticity of auditory cortex during appetitive operant conditioning. Biosystems, 101(1), 37–41. [PubMed: 20398726]

Takahashi H, Yokota R, Funamizu A, Kose H, & Kanzaki R (2011). Learning-stage-dependent, field-specific, map plasticity in the rat auditory cortex during appetitive operant conditioning. Neuroscience, 199, 243–258. [PubMed: 21985937]

Takesian AE, Kotak VC, & Sanes DH (2012). Age-dependent effect of hearing loss on cortical inhibitory synapse function. Journal of Neurophysiology, 107(3), 937–947. [PubMed: 22090457]

Taljaard DS, Olaithe M, Brennan-Jones CG, Eikelboom RH, & Bucks RS (2016). The relationship between hearing impairment and cognitive function: A meta-analysis in adults. Clinical Otolaryngology, 41(6), 718–729. [PubMed: 26670203]

Tervo DGR, Hwang BY, Viswanathan S, Gaj T, Lavzin M, Ritola KD, Lindo S, Michael S, Kuleshova E, Ojala D, Huang CC, Gerfen CR, Schiller J, Dudman JT, Hantman AW, Looger LL, Schaffer DV, & Karpova AY (2016). A Designer AAV Variant Permits Efficient Retrograde Access to Projection Neurons. Neuron, 92(2), 372–382. [PubMed: 27720486]

Treue S, & Maunsell JHR (1999). Effects of Attention on the Processing of Motion in Macaque Middle Temporal and Medial Superior Temporal Visual Cortical Areas. Journal of Neuroscience, 19(17), 7591–7602. [PubMed: 10460265]

Tucci DL, Cant NB, & Durham D (1999). Conductive Hearing Loss Results in a Decrease in Central Auditory System Activity in the Young Gerbil. The Laryngoscope, 109(9), 1359–1371. [PubMed: 10499037]

Vangkilde S, Coull JT, & Bundesen C (2012). Great expectations: Temporal expectation modulates perceptual processing speed. Journal of Experimental Psychology: Human Perception and Performance, 38, 1183–1191. [PubMed: 22250866]

Vanneste S, Joos K, & De Ridder D (2012). Prefrontal cortex based sex differences in tinnitus perception: Same tinnitus intensity, same tinnitus distress, different mood. PloS One, 7(2), e31182. [PubMed: 22348053]

Author Manuscript Author Manuscript Author Manuscript Author Manuscript

von Kriegstein K, Patterson RD, & Griffiths TD (2008). Task-Dependent Modulation of Medial Geniculate Body Is Behaviorally Relevant for Speech Recognition. Current Biology, 18(23–2), 1855–1859. [PubMed: 19062286]

von Trapp G, Aloni I, Young S, Semple MN, & Sanes DH (2017). Developmental hearing loss impedes auditory task learning and performance in gerbils. Hearing Research, 347, 3–10. [PubMed: 27746215]

von Trapp G, Buran BN, Sen K, Semple MN, & Sanes DH (2016). A Decline in Response Variability Improves Neural Signal Detection during Auditory Task Performance. Journal of Neuroscience, 36(43), 11097–11106. [PubMed: 27798189]

Wang X, Lu T, Bendor D, & Bartlett E (2008). Neural coding of temporal information in auditory thalamus and cortex. Neuroscience, 154(1), 294–303. [PubMed: 18555164]

Wetzel W, Wagner T, Ohl FW, & Scheich H (1998). Categorical discrimination of direction in frequency-modulated tones by Mongolian gerbils. Behavioural Brain Research, 91(1), 29–39. [PubMed: 9578437]

Williamson RS, & Polley DB (2019). Parallel pathways for sound processing and functional connectivity among layer 5 and 6 auditory corticofugal neurons. ELife, 8, e42974. [PubMed: 30735128]

Winer JA (2006). Decoding the auditory corticofugal systems. Hearing Research, 212(1), 1–8. [PubMed: 16555378]

Winkowski DE, Bandyopadhyay S, Shamma SA, & Kanold PO (2013). Frontal cortex activation causes rapid plasticity of auditory cortical processing Journal of Neuroscience, 33(46), 18134–18148. [PubMed: 24227723]

Winkowski DE, Nagode DA, Donaldson KJ, Yin P, Shamma SA, Fritz JB, & Kanold PO (2018). Orbitofrontal Cortex Neurons Respond to Sound and Activate Primary Auditory Cortex Neurons. Cerebral Cortex, 28(3), 868–879. [PubMed: 28069762]

Witter MP, Doan TP, Jacobsen B, Nilssen ES, & Ohara S (2017). Architecture of the Entorhinal Cortex A Review of Entorhinal Anatomy in Rodents with Some Comparative Notes. Frontiers in Systems Neuroscience, 11. https://www.frontiersin.org/articles/10.3389/fnsys.2017.00046

Xiong Q, Znamenskiy P, & Zador AM (2015). Selective corticostriatal plasticity during acquisition of an auditory discrimination task. Nature, 521(7552), 348–351. [PubMed: 25731173]

Xu H, Kotak VC, & Sanes DH (2007). Conductive Hearing Loss Disrupts Synaptic and Spike Adaptation in Developing Auditory Cortex. Journal of Neuroscience, 27(35), 9417–9426. [PubMed: 17728455]

Yao JD, Gimoto J, Constantinople CM, & Sanes DH (2020). Parietal Cortex Is Required for the Integration of Acoustic Evidence. Current Biology, 30(17), 3293–3303. [PubMed: 32619478]

Yao JD, & Sanes DH (2021). Temporal Encoding is Required for Categorization, But Not Discrimination. Cerebral Cortex, 31(6), 2886–2897. [PubMed: 33429423]

Yin P, Fritz JB, & Shamma SA (2014). Rapid Spectrotemporal Plasticity in Primary Auditory Cortex during Behavior. Journal of Neuroscience, 34(12), 4396–4408. [PubMed: 24647959]

Yin P, Strait DL, Radtke-Schuller S, Fritz JB, & Shamma SA (2020). Dynamics and Hierarchical Encoding of Non-compact Acoustic Categories in Auditory and Frontal Cortex. Current Biology, 30(9), 1649–1663. [PubMed: 32220317]

Yoshida T, & Katz DB (2011). Control of Prestimulus Activity Related to Improved Sensory Coding within a Discrimination Task. Journal of Neuroscience, 31(11), 4101–4112. [PubMed: 21411651]

Yotsumoto Y, & Watanabe T (2008). Defining a Link between Perceptual Learning and Attention. PLoS Biology, 6(8), e221. [PubMed: 18752357]

Young BJ, Otto T, Fox GD, & Eichenbaum H (1997). Memory Representation within the Parahippocampal Region. Journal of Neuroscience, 17(13), 5183–5195. [PubMed: 9185556]

Young JJ, & Shapiro ML (2011). Dynamic Coding of Goal-Directed Paths by Orbital Prefrontal Cortex. Journal of Neuroscience, 31(16), 5989–6000. [PubMed: 21508224]

Yu YQ, Xiong Y, Chan Y-S, & He J (2004). Corticofugal Gating of Auditory Information in the Thalamus: An In Vivo Intracellular Recording Study. Journal of Neuroscience, 24(12), 3060–3069. [PubMed: 15044545]

Author Manuscript Author Manuscript Author Manuscript Author Manuscript

Yun DH, Park YG, Cho JH, Kamentsky L, Evans NB, Albanese A, Xie K, Swaney J, Sohn CH, Tian Y, Zhang Q, Drummond G, Guan W, DiNapoli N, Choi H, Jung HY, Ruelas L, Feng G, & Chung K (2019). Ultrafast immunostaining of organ-scale tissues for scalable proteomic phenotyping (p. 660373). bioRxiv. 10.1101/660373

Zhang Y, Suga N, & Yan J (1997). Corticofugal modulation of frequency processing in bat auditory system. Nature, 387(6636), 900–903. [PubMed: 9202121]

Zhang Y, & Yan J (2008). Corticothalamic Feedback for Sound-Specific Plasticity of Auditory Thalamic Neurons Elicited by Tones Paired with Basal Forebrain Stimulation. Cerebral Cortex, 18(7), 1521–1528. [PubMed: 18203697]

Zingg B, Hintiryan H, Gou L, Song MY, Bay M, Bienkowski MS, Foster NN, Yamashita S, Bowman I, Toga AW, & Dong H-W (2014). Neural networks of the mouse neocortex. Cell, 156(5), 1096–1111. [PubMed: 24581503]

Znamenskiy P, & Zador AM (2013). Corticostriatal neurons in auditory cortex drive decisions during auditory discrimination. Nature, 497(7450), 482–485. [PubMed: 23636333]

Author Manuscript Author Manuscript Author Manuscript Author Manuscript

Orbitofrontal cortex may modulate changes in auditory processing. Using virally-mediated tracers, we found that projections from the orbitofrontal cortex to the auditory system primarily originate in the ventromedial subdivisions, preferentially target secondary auditory cortices and infragranular layers, and send axon collaterals to brain regions implicated in learning and memory.

Author Manuscript Author Manuscript Author Manuscript Author Manuscript

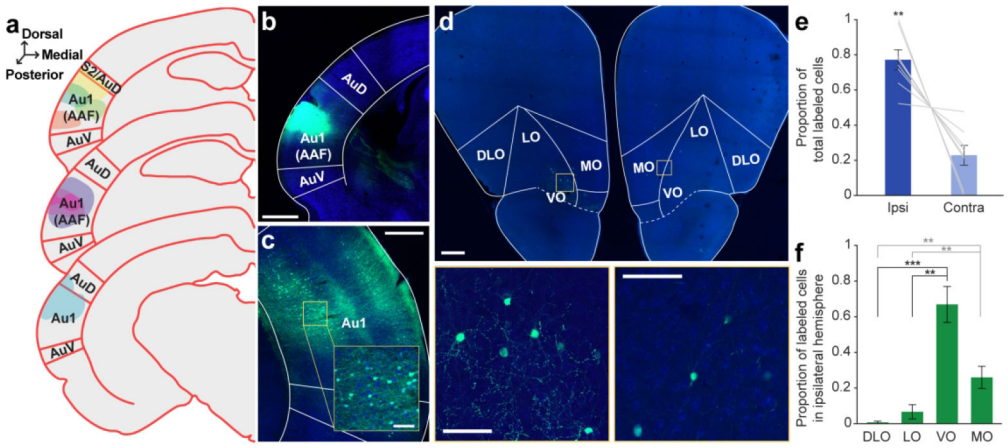

Figure 1. Retrograde tracer into Au1 reveals distinct profile of cell body labeling across the OFC mediolateral axis.

a. Schematic of all injection sites in Au1 (N = 8). Plate references from anterior to posterior: 29, 30, 32 (Radtke-Schuller et al., 2016). **b.** Injection site of representative subject. Scale bar = 1000 μm. **c.** In the same subject as B, expected labeling observed in the contralateral Au1. Scale bar = 500 μm, inset =100 μm. **d.** Representative OFC slice in the same subject as B. High magnification images depict cell bodies in the ipsilateral (left) and contralateral (right) hemispheres. Scale bar = 500 μm, high-mag = 100 μm. **e.** Proportion of total labeled cells in each hemisphere. Bars represent means ± standard error; lines connect data points from individual animals. **f.** Proportion of cell bodies within the ipsilateral hemisphere localized to each OFC subregion. Bars represent means ± standard error. **p<0.01, ***p<0.001.

Author Manuscript Author Manuscript Author Manuscript Author Manuscript

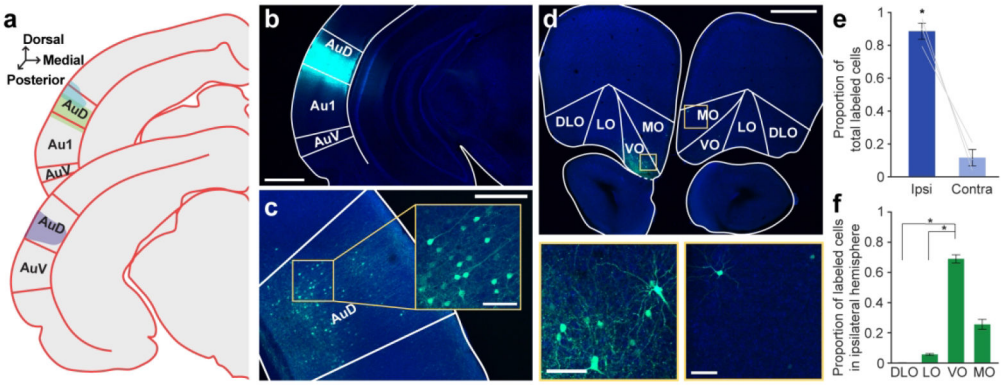

Figure 2. Retrograde tracer into AuD labels cell bodies in OFC.

a. Schematic of all injection sites in left AuD (N = 3). Plate references from anterior to posterior: 33, 34 (Radtke-Schuller et al., 2016). **b.** Injection site of representative subject. Scale bar = 1000 μm. **c.** In the same subject as in B, expected labeling observed in contralateral AuD. Scale bar = 500 μm, inset =100 μm. **d.** Labeled OFC cell bodies in the same subject as B. High magnification images depict cell bodies in the ipsilateral (left) and contralateral (right) OFC. Scale bar = 500 μm, high-mag = 100 μm. **e.** Proportion of total labeled cells in each hemisphere. Bars represent means ± standard error; lines connect data points from individual animals. **f.** Proportion of cell bodies within the ipsilateral hemisphere localized to each OFC subregion. Bars represent means ± standard error. *p<0.05

Author Manuscript Author Manuscript Author Manuscript Author Manuscript

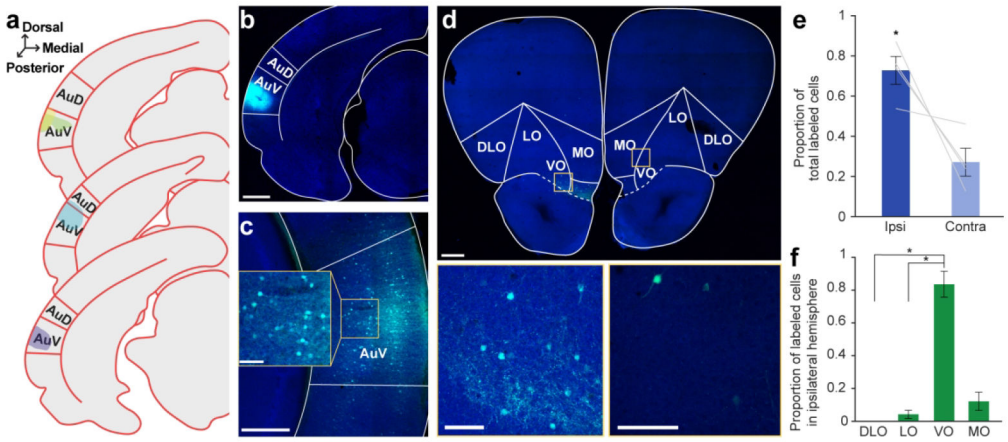

Figure 3. Retrograde tracer into AuV labels cell bodies in OFC.

a. Schematic of all injection sites in left AuV (N = 4). Plate references from anterior to posterior: 34, 35, 36 (Radtke-Schuller et al., 2016). **b.** Injection site of representative subject. Scale bar = 1000 μm. **c.** In the same subject as in B, expected labeling observed in contralateral AuV. Scale bar = 500 μm, inset =100 μm. **d.** Labeled OFC cell bodies in the same subject as B. High magnification images depict cell bodies in the ipsilateral (left) and contralateral (right) OFC. Scale bar = 500 μm, insets = 100 μm. **e.** Proportion of total labeled cells in each hemisphere. Bars represent means ± standard error; lines connect data points from individual animals. **f.** Proportion of cell bodies within the ipsilateral hemisphere localized to each OFC subregion. Bars represent means ± standard error. *p<0.05

Author Manuscript Author Manuscript Author Manuscript Author Manuscript

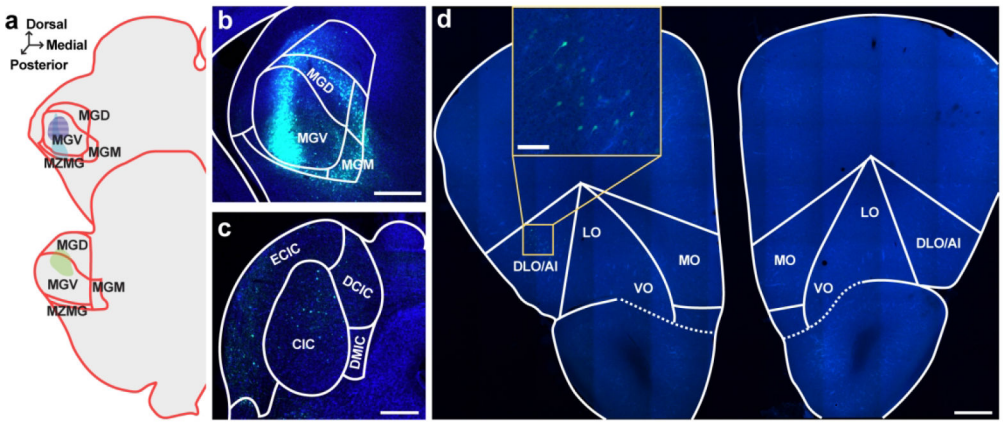

Figure 4. Retrograde tracer into MGN sparsely labels cell bodies in OFC.

a. Schematic of all injection sites in MGN (N = 3). Plate references from anterior to posterior: 34, 35 (Radtke-Schuller et al., 2016). Striped pattern denotes an injection that resulted in no observed cell body labeling in the OFC. **b.** Injection site of representative subject. Scale bar = 500 μm. **c.** In the same subject as B, expected labeling observed in IC. Scale bar = 500 μm. **d.** Representative OFC slice in the same subject as B. Scale bar = 500 μm, inset =100 μm.

Author Manuscript Author Manuscript Author Manuscript Author Manuscript

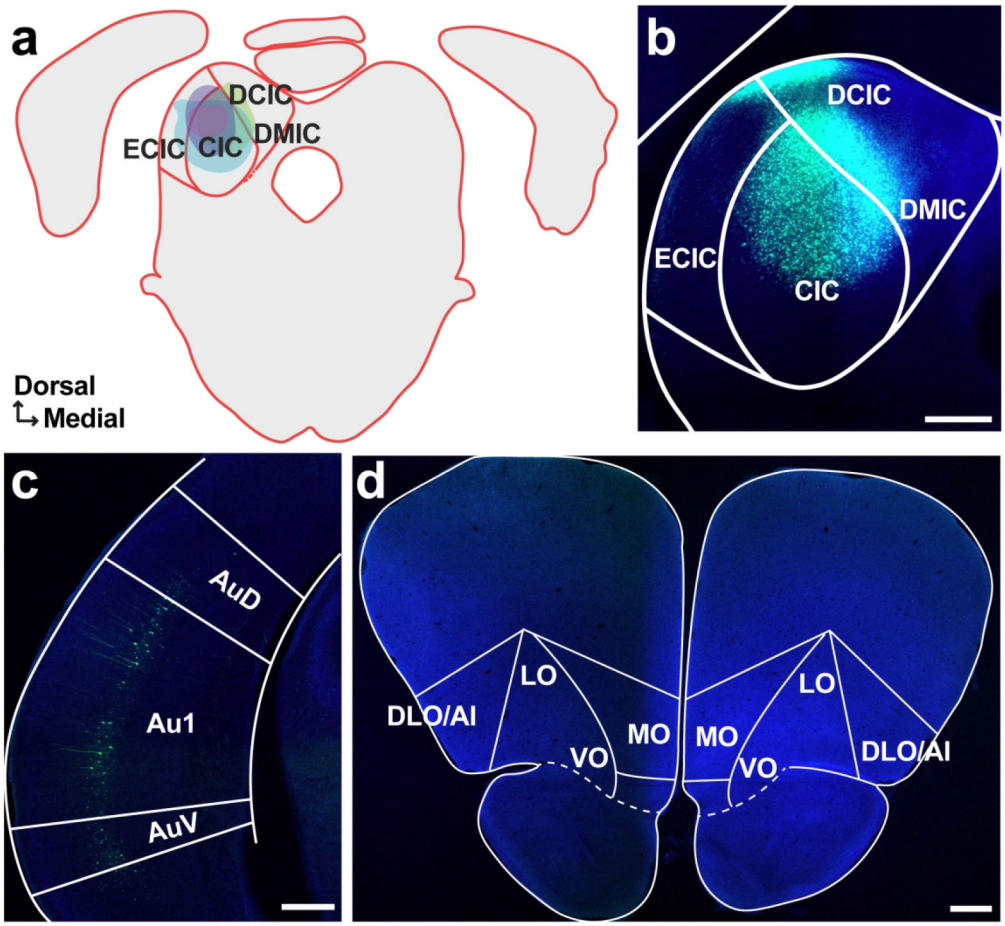

Figure 5. Retrograde tracer into IC does not label cell bodies in OFC.

a. Schematic of all injection sites in IC (N = 3). Plate reference: 42 (Radtke-Schuller et al., 2016) **b.** Injection site of representative subject. Scale bar = 500 μm. **c.** Expected labeling observed in Au1. Scale bar = 500 μm. **d.** Representative OFC slice in the same subject as B showing no cell bodies. Scale bar = 500 μm.

Author Manuscript Author Manuscript Author Manuscript Author Manuscript

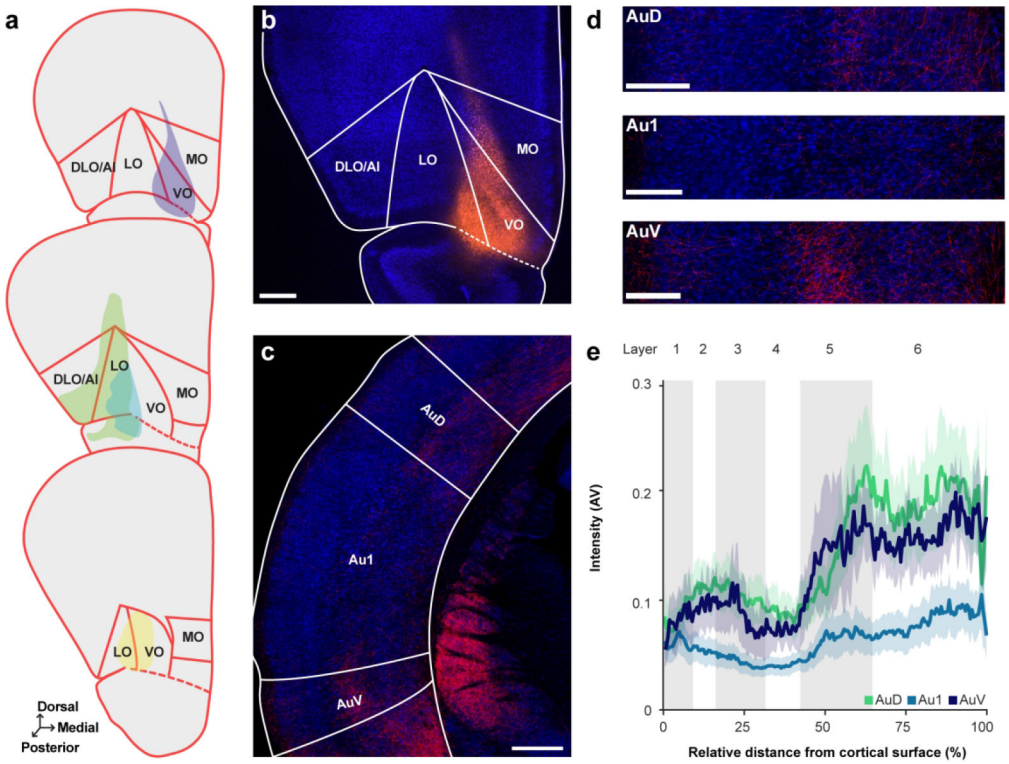

Figure 6. Anterograde tracer into OFC reveals region- and layer-specific innervation pattern in auditory cortex.

a. Schematic of all injection sites in OFC (N = 4). Plate references from anterior to posterior: 11, 12, 13 (Radtke-Schuller et al., 2016). **b.** Injection site of representative subject. Scale bar = 500 μm. **c.** Labeled terminals in the auditory cortex. Scale bar = 500 μm. **d.** From the same subject as in C, close-up images of terminals through AuD (top), Au1 (middle), and AuV (bottom). Scale bars = 250 μm. **e.** Normalized label intensity (arbitrary value, AV) for each subregion as a function of relative distance from the cortical surface. Lines represent means across animals; shading represents standard error.

Author Manuscript Author Manuscript Author Manuscript Author Manuscript

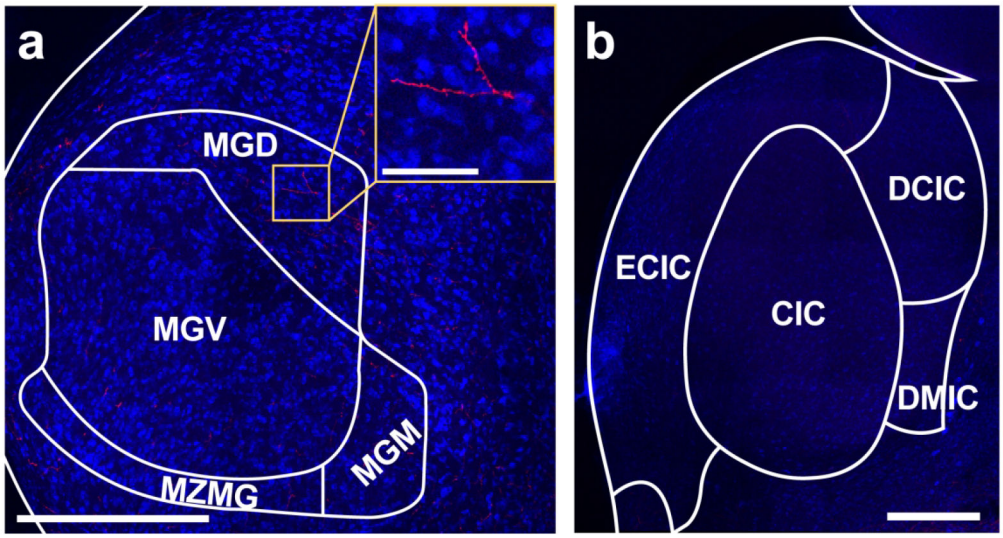

Figure 7. Anterograde tracer into OFC reveals sparse fiber labeling in MGN.

a. Sparse labeling observed in the MGN in subjects with anterograde tracers injected into the OFC. Scale bar = 500 μm, inset = 100 μm. **b.** No labeling was observed in the IC. Scale bar = 500 μm.

Author Manuscript Author Manuscript Author Manuscript Author Manuscript

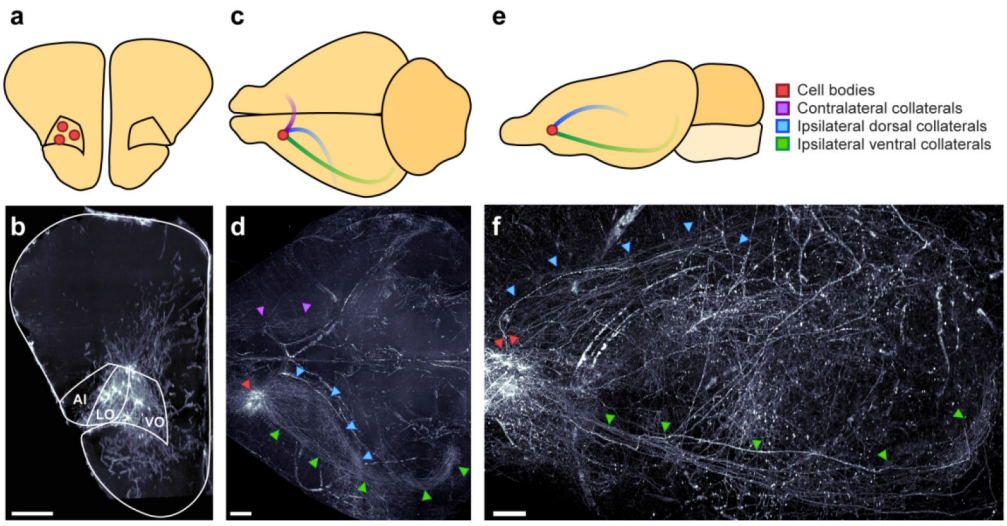

Figure 8. OFC neurons that project to auditory cortex send axon collaterals to other brain regions.

a-b. Coronal schematic (**a**) and section (**b**) depicting location of identified cell bodies in a representative subject. Section is a 175 μm thick coronal z-stack. Scale bar = 500 μm. **c-d.** Horizontal schematic (**c**) and view (**d**) depicting notable axon tracts emanating from OFC neurons in a representative subject. Scale bar = 1000 μm. **e-f.** Sagittal view (**e**) and section (**f**) depicting axon tracts in representative subject. Scale bar = 1000 μm.

Author Manuscript Author Manuscript Author Manuscript Author Manuscript

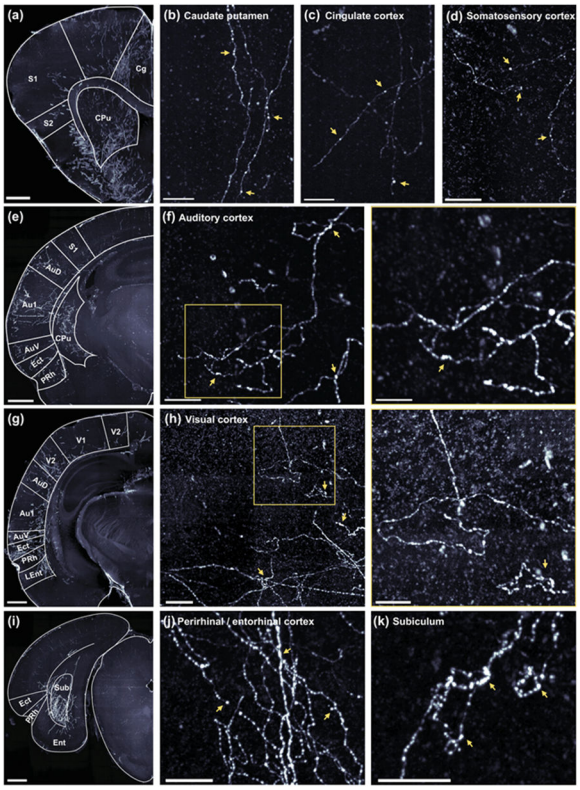

Figure 9. OFC neurons that project to auditory cortex exhibit synaptic boutons in many non-auditory brain regions.

a-d. Low magnification (**a**) and high magnification (**b-d**) images depicting labeled axon fibers in the anterior caudate putamen (**b**), cingulate cortex (**c**) and the somatosensory cortex (**d**). In b-d, scale bar = 100 μm. Here, and in all following panels, yellow arrows highlight likely synaptic boutons. **e.** Low magnification image depicting labeled axon fibers in the anterior auditory cortex, parahippocampal region, and caudate putamen. **f.** High magnification images depicting labeled axon fibers in the auditory cortex. Scale bars = 100 μm (left), and 50 μm (right). **g.** Low magnification image depicting labeled axon fibers in visual cortex, posterior auditory cortex, and the parahippocampal region. **h.** High magnification images depicting labeled axon fibers in the visual cortex. Scale bars = 100 μm (left), and 50 μm (right). **I.** Low magnification image depicting labeled axon fibers in the subiculum translational area. **j-k.** High magnification images depicting labeled axons fibers in the perirhinal and entorhinal cortices (**j**) and the subiculum (**k**). Scale bars = 50 μm. In panels a, e, g, and i, images are 175 μm thick coronal z-stacks with 1000 μm scale bars.

Author Manuscript Author Manuscript Author Manuscript Author Manuscript

Table 1.

Subjects and injection coordinates. Pipette angle = 0° unless otherwise noted. * denotes representative subject used for figure.

Subject	Sex	Age (days)	Injection site	Virus	Coordinates (mm) ML, from lambda, unless otherwise noted RC, from lambda DV, from pial surface	Volume (nL)	Titer (GC/mL)
ID_269953	M	58	OFC	AAV1/pENN.AAV.hSyn.TurboRFP.WPRE.RBG (Addgene 105552)	−1.5 ML, 8.75 RC, −3.5 DV	90	2.6 x 10^{14}
SUBJ-ID-122	M	365	OFC	AAV1/pENN.AAV.hSyn.TurboRFP.WPRE.RBG (Addgene 105552)	−1.5 ML, 8.94 RC, −3.2 DV	150	1.5 x 10^{13}
SUBJ-ID-123*	M	365	OFC	AAV1/pENN.AAV.hSyn.TurboRFP.WPRE.RBG (Addgene 105552)	−1.5 ML, 8.95 RC, −3.2 DV	100	1.5 x 10^{13}
SUBJ-ID-294*	F	230	OFC	AAV1/pENN.AAV.hSyn.TurboRFP.WPRE.RBG (Addgene 105552)	−1.2 ML, 9.45 RC, −3.2 DV	80	1.5 x 10^{13}
SUBJ-ID-353*	F	271	AuD	AAVrg/pAAV-hSyn-EGFP (Addgene 50465)	−6.4 ML, 1.05 RC, −0.9 DV	200	1.7 x 10^{13}
					−6.4 ML, 1.05 RC, −0.45 DV 45° M-L	200	
SUBJ-ID-354	F	271	AuD	AAVrg/pAAV-hSyn-EGFP (Addgene 50465)	−6.45 ML, 1.05 mm RC, −0.9 DV	200	1.7 x 10^{13}
					−6.45 ML, 1.05 mm RC, −0.45 DV 45° M-L	200	
SUBJ-ID-355	F	271	AuD	AAVrg/pAAV-hSyn-EGFP (Addgene 50465)	−1.25 ML from temporal ridge, 1.34 RC, −0.9 DV	200	1.7 x 10^{13}
					−1.25 ML from temporal ridge, 1.34 RC, −0.45 DV 45° M-L	100	
SUBJ-ID-56	M	233	Au1	AAVrg/pAAV-hSyn-EGFP (Addgene 50465)	−1.4 ML from temporal ridge, 3.5 RC, −0.75 DV	200	1 x 10^{13}
					−1.4 ML from temporal ridge, 3.5 RC, −0.35 DV 45° M-L	200	
SUBJ-ID-110	F	637	Au1	AAVrg/pAAV-hSyn-EGFP (Addgene 50465)	−1 ML from temporal ridge, 3.5 RC, −0.9 DV	200	1 x 10^{13}
					−1 ML from temporal ridge, 3.5 RC, −0.45 DV 45° M-L	200	
SUBJ-ID-111	F	637	Au1	AAVrg/pAAV-hSyn-EGFP (Addgene 50465)	−1 ML from temporal ridge, 3.45 RC, −0.9 DV	200	1 x 10^{13}

Author Manuscript Author Manuscript Author Manuscript Author Manuscript

Subject	Sex	Age (days)	Injection site	Virus	Coordinates (mm) ML, from lambda, unless otherwise noted RC, from lambda DV, from pial surface	Volume (nL)	Titer (GC/mL)
					−1 ML from temporal ridge, 3.45 RC, −0.45 DV 45° M-L	200	
SUBJ-ID-121	M	365	Au1	AAVrg/pAAV-hSyn-EGFP (Addgene 50465)	−1 ML from temporal ridge, 3.3 RC, −0.75 DV	200	1 x 10^{13}
					−1 ML from temporal ridge, 3.3 RC, −0.35 DV 45° M-L	200	
SUBJ-ID-133	F	328	Au1	AAVrg/pAAV-hSyn-EGFP (Addgene 50465)	−1 ML from temporal ridge, 3.5 RC, −0.75 DV	200	1 x 10^{13}
					−1 ML from temporal ridge, 3.5 RC, −0.35 DV	200	
SUBJ-ID-297	F	263	Au1	AAVrg/pAAV-hSyn-EGFP (Addgene 50465)	−1 ML from temporal ridge, 3.5 RC, −0.75 DV	200	1 x 10^{13}
					−1 ML from temporal ridge, 3.5 RC, −0.35 DV	200	
SUBJ-ID-298*	F	181	Au1	AAVrg/pAAV-hSyn-EGFP (Addgene 50465)	−1.05 ML from temporal ridge, 3.5 RC, −0.9 DV	200	1.7 x 10^{13}
					−1.05 ML from temporal ridge, 3.5 RC, −0.45 DV 30° M-L	200	
SUBJ-ID-299	F	181	AuV	AAVrg-CAG-tdTomato (Addgene 59462)	−1.25 ML from temporal ridge, 1.34 RC, −0.9 DV	200	2.5 x 10^{13}
					−1.25 ML from temporal ridge, 1.34 RC, −0.45 DV 45° M-L	200	
SUBJ-ID-300	F	181	Au1	AAVrg/pAAV-hSyn-EGFP (Addgene 50465)	−1.25 ML from temporal ridge, 3.55 RC, −0.9 DV	200	1 x 10^{13}
			AuV	AAVrg-CAG-tdTomato (Addgene 59462)	−1.25 ML from temporal ridge, 3.55 RC, −0.45 DV	200	
					−1.25 ML from temporal ridge, 1.34 RC, −0.9 DV	200	2.5 x 10^{13}
					−1.25 ML from temporal ridge, 1.34 RC, −0.45 DV 45° M-L	200	

Author Manuscript Author Manuscript Author Manuscript Author Manuscript

Subject	Sex	Age (days)	Injection site	Virus	Coordinates (mm) ML, from lambda, unless otherwise noted RC, from lambda DV, from pial surface	Volume (nL)	Titer (GC/mL)
SUBJ-ID-391	M	346	AuV	AAVrg/pAAV-hSyn-EGFP (Addgene 50465)	−8.0 ML, 1.38 RC, −0.9 DV	200	1.7 x 10^{13}
					−8.0 ML, 1.38 RC, −0.45 DV 45° M-L	200	
SUBJ-ID-392	M	346	AuV	AAVrg/pAAV-hSyn-EGFP (Addgene 50465)	−8.0 ML, 1.35 RC, −0.9 DV	200	1.7 x 10^{13}
					−8.0 ML, 1.35 RC, −0.45 DV 45° M-L	200	
SUBJ-ID-126	F	605	MGV	AAVrg/pAAV-hSyn-EGFP (Addgene 50465)	−3 ML ,1.5 RC, −4.15 DV	50	1 x 10^{13}
SUBJ-ID-180*	M	489	MGV	AAVrg/pAAV-hSyn-EGFP (Addgene 50465)	−2.85 ML, 1.75 RC, −4.15 DV	80	1 x 10^{13}
SUBJ-ID-181	M	489	MGV	AAVrg/pAAV-hSyn-EGFP (Addgene 50465)	−2.85 ML, 1.75 RC, −4.18 DV	80	1 x 10^{13}
SUBJ-ID-95	M	408	CIC	AAVrg/pAAV-hSyn-EGFP (Addgene 50465)	−1.65 ML, 0.35 RC, −3.65 DV	80	1 x 10^{13}
					30° R-C		
SUBJ-ID-119	F	396	CIC	AAVrg/pAAV-hSyn-EGFP (Addgene 50465)	−1.65 ML, 0.35 RC, −3.65 DV	200	1 x 10^{13}
					30° R-C		
SUBJ-ID-120	F	396	CIC	AAVrg/pAAV-hSyn-EGFP (Addgene 50465)	−1.65 ML, 0.35 RC, −3.65 DV	80	1 x 10^{13}
					30° R-C		
SUBJ-ID-124*	M	396	CIC	AAVrg/pAAV-hSyn-EGFP (Addgene 50465)	−1.65 ML, 0.35 RC, −3.65 DV	150	1 x 10^{13}
					30° R-C		
SUBJ-ID-143	F	442	OFC Au1	AAV1-hSyn-DIO-mCherry (Addgene 50459) AAVrg-hSyn-Cre-WPRE.HGH (Addgene 105553)	−1.5 ML, 9.05 RC, −2.75 DV	100	9 x 10^{18}
					1.35 ML from temporal ridge, 3.55 RC, −0.75 DV	200	1.2 x 10^{13}
					1.35 ML from temporal ridge, 3.55 RC, −0.35 DV	200	
					1.35 ML from temporal ridge, 3.7 RC, −0.75 DV	200	
					1.35 ML from temporal ridge, 3.7 RC, −0.35 DV	200	
SUBJ-ID-144	F	442	OFC Au1	AAV1-hSyn-DIO-mCherry (Addgene 50459) AAVrg-hSyn-Cre-WPRE.HGH (Addgene 105553)	−1.5 ML, 9.05 RC, −2.75 DV	100	9 x 10^{18}
					1.35 ML from temporal ridge, 3.2 RC, −0.75 DV	200	1.2 x 10^{13}

Author Manuscript

Author Manuscript

Author Manuscript

Author Manuscript

Subject	Sex	Age (days)	Injection site	Virus	Coordinates (mm) ML, from lambda, unless otherwise noted RC, from lambda DV, from pial surface	Volume (nL)	Titer (GC/mL)
					1.35 ML from temporal ridge, 3.2 RC, −0.35 DV	200	
					1.35 ML from temporal ridge, 3.9 RC, −0.75 DV	200	
					1.35 ML from temporal ridge, 3.9 RC, −0.35 DV	200s	

Author Manuscript Author Manuscript Author Manuscript Author Manuscript

Table 2.

Raw OFC cell count data. Plate reference refers to the plate number in the gerbil brain atlas (Radtke-Schuller et al., 2016).

Subject	Injection site	Ipsi plate reference	Contra plate reference	DLO (Ipsi)	LO (Ipsi)	VO (Ipsi)	MO (Ipsi)	DLO (Contra)	LO (Contra)	VO (Contra)	MO (Contra)
SUBJ-ID-353	AuD	10	10	0	0	4	2	0	0	0	0
		10	10	0	0	26	5	0	0	0	1
		11	11	0	1	30	6	0	0	1	4
		12	11	0	0	16	22	0	0	5	4
		12	12	1	0	19	16	0	0	3	9
		12	12	0	1	31	9	0	1	7	2
		12	12	0	1	12	8	0	0	9	3
		13	13	--	2	1	3	--	0	2	2
		14	13	--	3	6	3	--	0	0	3
		15	15	--	3	14	--	--	4	4	--
SUBJ-ID-354	AuD	10	10	0	0	1	5	0	0	0	0
		10	10	0	0	11	1	0	0	0	0
		11	11	0	3	25	2	0	0	0	0
		11	11	0	0	14	4	0	0	0	0
		12	12	0	0	15	3	0	0	1	1
		13	13	--	0	7	3	--	0	0	0
		13	13	--	0	0	0	--	0	1	1
		14	14	--	4	2	0	--	0	0	0
SUBJ-ID-355	AuD	10	10	0	0	25	2	0	0	0	0
		11	11	0	7	16	10	0	0	2	3
		12	12	0	2	39	16	0	0	1	5
		12	12	0	0	22	12	0	0	3	0
		13	13	--	0	2	3	--	0	4	0
		14	14	--	0	2	2	--	0	0	0
		14	14	--	0	0	0	--	0	0	0
SUBJ-ID-56	Au1	12	12	0	0	14	1	0	0	4	0
		14	14	0	0	3	0	0	0	1	2
SUBJ-ID-110	Au1	12	12	0	6	9	40	4	5	5	44
		13	13	--	2	14	14	--	0	12	25
		14	14	--	12	15	27	--	8	1	25
		15	15	--	16	13	--	--	21	3	--
SUBJ-ID-111	Au1	10	10	3	5	14	7	0	3	6	1
		10	10	0	2	8	7	0	1	2	1
		11	11	0	5	11	6	0	1	10	0
		12	12	1	2	25	16	2	3	3	1

Author Manuscript Author Manuscript Author Manuscript Author Manuscript

Subject	Injection site	Ipsi plate reference	Contra plate reference	DLO (Ipsi)	LO (Ipsi)	VO (Ipsi)	MO (Ipsi)	DLO (Contra)	LO (Contra)	VO (Contra)	MO (Contra)
		12	12	1	6	26	9	0	2	13	0
		13	13	--	1	11	2	--	1	1	0
		14	14	--	3	12	1	--	1	0	1
SUBJ-ID-121	Au1	10	10	0	0	4	2	0	0	0	0
		11	11	0	0	8	1	0	0	2	4
		12	12	0	0	6	2	0	0	2	0
SUBJ-ID-133	Au1	10	10	0	0	7	1	0	0	0	0
		10	11	0	0	10	6	0	0	0	0
		12	12	0	0	13	3	0	0	1	0
		12	12	0	1	13	1	0	0	0	0
SUBJ-ID-297	Au1	9	9	0	0	0	0	0	0	0	0
		10	10	0	0	0	1	0	0	0	0
		10	10	0	0	0	1	0	0	1	0
		11	11	0	0	5	2	0	0	0	0
		11	11	0	1	5	5	0	1	1	3
		12	12	0	2	10	6	0	6	6	2
		13	13	--	0	18	2	--	2	6	3
		14	14	--	0	5	1	--	2	3	0
SUBJ-ID-298	Au1	11	11	0	5	12	10	0	1	0	2
		12	12	2	1	14	8	0	1	2	5
		12	13	0	2	7	6	--	1	3	3
SUBJ-ID-300	Au1	11	11	0	0	0	0	0	0	0	0
		11	11	0	0	1	1	0	0	0	0
		12	12	0	0	2	0	0	0	0	0
		13	13	--	0	3	1	--	0	0	0
		14	14	--	0	1	0	--	0	0	0
SUBJ-ID-299	AuV	12	12	0	0	7	0	0	0	8	0
		14	14	--	0	7	0	--	0	4	0
SUBJ-ID-300	AuV	11	11	0	0	1	2	0	0	0	0
		11	11	0	0	3	1	0	0	0	1
		12	12	0	1	4	0	0	0	0	0
		13	13	--	0	16	0	--	0	1	0
		14	14	--	0	13	0	--	0	4	0
SUBJ-ID-391	AuV	10	10	0	0	0	1	0	0	0	0
		10	10	0	0	0	1	0	0	0	0
		10	10	0	0	0	1	0	0	0	1
		11	11	0	0	1	2	0	0	0	0
		11	11	0	0	9	3	0	0	0	3

Author Manuscript Author Manuscript Author Manuscript Author Manuscript

Subject	Injection site	Ipsi plate reference	Contra plate reference	DLO (Ipsi)	LO (Ipsi)	VO (Ipsi)	MO (Ipsi)	DLO (Contra)	LO (Contra)	VO (Contra)	MO (Contra)
		12	12	0	0	12	1	0	3	4	0
		14	14	--	0	0	0	--	0	0	0
		16	16	--	4	0	--	--	0	0	--
SUBJ-ID-392	AuV	9	9	0	0	0	1	0	0	0	0
		10	10	0	0	2	0	0	0	0	0
		10	10	0	0	1	1	0	0	0	0
		11	11	0	0	11	3	0	0	2	3
		11	12	0	0	22	4	0	0	5	2
		12	12	0	0	4	3	0	0	0	0
		13	13	--	0	28	1	--	0	13	1
		14	14	--	0	5	2	--	0	0	4
		15	15	--	0	0	--	--	0	0	--
		15	15	--	3	4	--	--	0	3	--

Author Manuscript

Author Manuscript

Author Manuscript

Author Manuscript

Table 3.

Paired t-tests comparing proportion of labeled cell bodies in each OFC subregion after retrograde injections into Au1 (see Figure 1). All p-values were corrected for multiple comparisons using a Bonferroni adjustment.

Subregion comparison	t ratio	p-value
VO - MO	3.556	0.0558
VO – LO	6.088	0.003**
VO – DLO	8.987	0.0001**
MO – LO	7.880	0.0006**
MO – DLO	5.879	0.0036**
LO – DLO	2.229	0.3666

Author Manuscript

Author Manuscript

Author Manuscript

Author Manuscript

Table 4.

Paired t-tests comparing proportion of labeled cell bodies in each OFC subregion after retrograde injection into AuD (see Figure 2). All p-values were corrected for multiple comparisons using a Bonferroni adjustment.

Subregion comparison	t ratio	p-value
VO - MO	6.240	0.1482
VO – LO	25.252	0.0096*
VO – DLO	21.102	0.0132*
MO – LO	4.419	0.2856
MO – DLO	6.867	0.1236
LO – DLO	6.607	0.1332

Author Manuscript

Author Manuscript

Author Manuscript

Author Manuscript

Table 5.

Paired t-tests comparing proportion of labeled cell bodies in each OFC subregion after retrograde injection into AuV (see Figure 3). All p-values were corrected for multiple comparisons using a Bonferroni adjustment.

Subregion comparison	t ratio	p-value
VO - MO	5.314	0.0780
VO – LO	7.678	0.0276*
VO – DLO	10.568	0.0108*
MO – LO	2.373	0.5898
MO – DLO	2.203	0.6888
LO – DLO	1.713	1.0000

Author Manuscript

Author Manuscript

Author Manuscript

Author Manuscript

Table 6.

Paired t-tests comparing intensity of labeled OFC axon fibers across auditory cortical layers (see Figure 6). All p values were corrected for multiple comparisons using a Bonferroni adjustment.

Layer comparison	t ratio	p-value
1 - 2	−1.504	1.0000
1 – 3	−0.333	1.0000
1 – 4	0.894	1.0000
1 – 5	−3.974	0.0020**
1 – 6	−5.094	< 0.0001***
2 – 3	1.198	1.0000
2 – 4	2.259	0.3901
2 – 5	−3.134	0.0337*
2 – 6	−4.666	0.0001**
3 – 4	1.210	1.0000
3 – 5	−3.824	0.0034**
3 – 6	−5.021	< 0.0001***
4 – 5	−4.310	0.0006**
4 – 6	−5.249	< 0.0001***
5 – 6	−2.599	0.1609

Author Manuscript Author Manuscript Author Manuscript Author Manuscript

Table 7.

Qualitative estimate of the intensity of labeled fibers in various brain regions innervated by OFC-Au1 axon collaterals. (+): weak labeling, (++): moderate labeling, (+++): dense labeling.

Region	Intensity
Anterior olfactory nucleus (dorsal)	++
Anterior olfactory nucleus (lateral)	++
Anterior olfactory nucleus (posterior)	++
Amygdala	
Central amygdaloid nucleus	+
Lateral amygdaloid nucleus	+
Medial amygdaloid nucleus	+
Caudate putamen	+++
Claustrum	+
Cortex	
Agranular insular	+
Auditory (primary)	+++
Auditory (secondary, dorsal)	+++
Auditory (secondary, ventral)	+++
Cingulate	++
Dorsal peduncular	+
Ectorhinal	+++
Entorhinal	++
Motor (primary)	+
Motor (secondary)	++
Parietal	+
Perirhinal	++
Piriform	+
Prelimbic	++
Orbitofrontal (dorsolateral)	+
Orbitofrontal (medial)	+++
Orbitofrontal (lateral)	+++
Orbitofrontal (ventral)	+++
Retrosplenial	++
Somatosensory (primary)	+
Somatosensory (secondary)	+
Visual (primary)	+
Visual (secondary)	+
Dorsal endopiriform nucleus	+
Nucleus accumbens (core)	+++
Nucleus accumbens (shell)	+++

Author Manuscript

Author Manuscript

Author Manuscript

Author Manuscript

Region	Intensity
Subiculum	
Parasubiculum	++
Postsubiculum	++
Subiculum, transitional area	+++